ACS OMEGA

http://pubs.acs.org/journal/acsodf

Article

Photoluminescent Thin Films of Room-Temperature Glassy Tris(keto-hydrozone) Discotic Liquid Crystals and Their Nanocomposites with Single-Walled Carbon Nanotubes for Optoelectronics

Georgi B. Hadjichristov* and Yordan G. Marinov

Cite This: *ACS Omega* 2023, 8, 27102−27116

Read Online

ACCESS | Metrics & More | Article Recommendations | Supporting Information

ABSTRACT: This study addresses the photoresponse of liquid-crystalline tris(keto-hydrozone) discotic (TKHD)—a star-shaped molecular structure with three branches. Object of our research interest was also TKHD filled with single-walled carbon nanotubes (SWCNTs) at a concentration of 1 wt %. At room temperature, the discotic liquid crystals in thin films (thickness 3 μm) of both TKHD and nanocomposite SWCNT/TKHD were in a glassy state. Such glassy thin films exhibited photoluminescence ranging from the deep-red to the near-infrared spectral region, being attractive for organic optoelectronics. The addition of SWCNTs to TKHD was found to stabilize the photoluminescence of TKHD, which is of significance for optoelectronic device applications. The photothermoelectrical response of highly conductive SWCNT/TKHD nanocomposite films was characterized by electrical impedance spectroscopy in the frequency range from 1 Hz to 1 MHz of the applied electric field. It was elucidated that the reversible photothermoelectrical effect in SWCNT/TKHD films occurs through SWCNTs and their network.

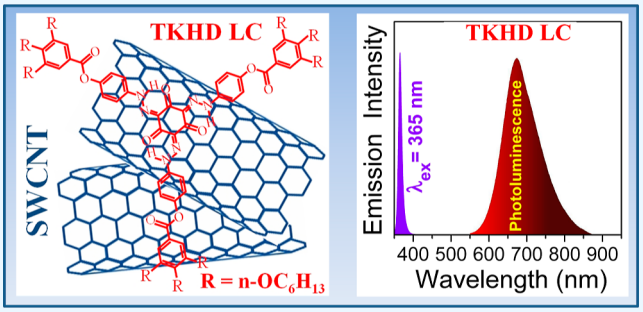

1. INTRODUCTION

Organic semiconducting media of disk-shaped molecules that spontaneously self-assemble into a stable liquid-crystalline (LC) phase over a wide thermal range[1,2] are technically significant materials for use in nanoscale (opto)electronically active components and electronic devices, such as organic light-emitting devices (OLEDs) and emissive wide-viewing LC displays,[3] organic field-effect transistors,[4] as well as in organic photovoltaics (OPVs).[5] The molecules of discotic liquid crystals (DLCs),[6−12] an important class of liquid crystals, have sizes ranging from 2 to 6 nm and form nanostructured organic soft media. These materials have been attracting special attention in the last decade and, currently, gain increased research and application interest because they combine the unique feature of self-assembly and functional optical, electronic, thermal, photoluminescent, fluorescent, and other properties, useful for organo-electronics, non-linear optics, and photonics, OPVs, bio-imaging, sensorics, mechatronics, and other advanced applications.[8,11−14] Various DLCs, functionalized DLCs, and DLC polymers are highly conjugated organic semiconductors and photoresponsive materials.[14,15] They have important physical and chemical properties that determine wide areas of their practical application. Currently, novel multifunctional DLC materials are extensively synthesized, comprehensively studied, and used for design of active organic media in various fields of science and technology, in particular, soft electronics, flexible electronics, and optoelectronics.[16,17]

By inclusion of highly conductive nanoparticles in DLC materials, e.g., gold, silver, or other metallic nanoparticles, as well as carbon nanostructures, e.g., carbon nanotubes (CNTs),[18,19] one can design nanocomposites (NCs) with enhanced electrical conductivity and other valuable properties, keeping the LC behavior of the NCs. In relevant applications, the combination of DLCs and nanomaterials is advantageous.[20−22] In the development of advanced multifunctional NCs, of special interest are the single wall CNTs (SWCNTs), due to their unique mechanical, thermal, and electrical properties. These prospective nanomaterials and their networks composed of either aligned or disordered SWCNT assemblies have a wide application in nanoscale-sized organic microelectronics, optoelectronics, and photonics, OPVs, and sensorics, among others.[23] Importantly, CNT fillers have a

Received: March 29, 2023
Accepted: July 6, 2023
Published: July 18, 2023

https://doi.org/10.1021/acsomega.3c02103
ACS Omega 2023, 8, 27102−27116

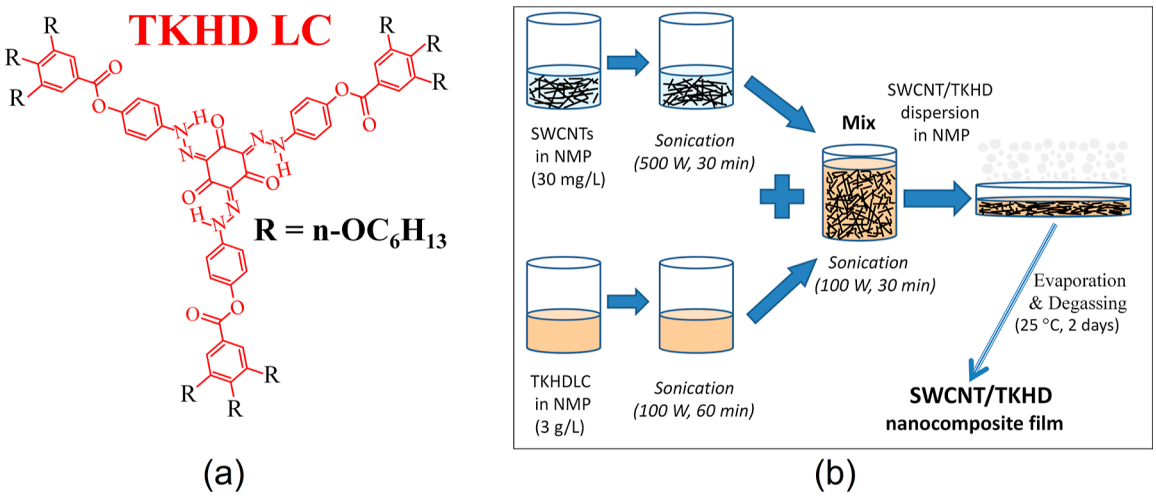

Figure 1. (a) Molecular structure of TKHDLC and (b) schematic representation of the fabrication steps of SWCNTs/TKHD NC.

great potential for desirable change of the thermal stability, mechanical, dielectric, and other valuable properties of the NC soft materials. In recent years, such high-performance multicomponent NCs, hybrid and metamaterials gain a lot of attention directed toward the improvement of the existing technologies such as flexible sensor and mechatronic systems, catalysis, production of novel flexible miniature electronic and dielectric devices for flexible and portable electronics, and for use in stretchable, wearing, and printed electronics, as well as in electromagnetic shielding and flame retardant, expanding their applicability and functionality.[24] One of the intriguing properties of SWCNTs and SWCNT networks is their thermoelectric response, attractive for large-scale thermal energy applications.[25] At present, the employment of SWCNT/DLC NCs in the application fields of organic semiconductors is challenging[26] and has yet to be widely explored.

Star-shaped DLCs having a disk-like core with three branches[27,28] have demonstrated very interesting electronic and luminescent response useful for diverse applications.[29] By doping of such materials with CNTs, one can produce highly conductive DLC NCs that exhibit enhanced properties, e.g., improved light emissive and sensing characteristics. Very recently, we have studied the photo-electrical response of thin films of NCs based on star-shaped tris(keto-hydrozone) dicotics with six carbon atoms in the tails (hereafter abbreviated as TKHDLC or shortly TKHD), filled with SWCNTs.[30] As the neat TKHD, the SWCNTs/TKHD NCs can form a "glassy"-like columnar state that takes place in a large temperature range including the room temperatures (16−40 °C).[31] The practical importance of glassy DLC films for robust optoelectronic devices is well established.[32] Notably, the glassy state of DLCs, which have a molecular structure of the type similar to that of TKHD, exhibits interesting luminescence behavior at room temperature.[27] In the present work, our research interest was focused on the photoresponse of glassy thin films of TKHD and TKHD filled with SWCNTs, especially on the photo-induced changes of their photoluminescence (PL) that are relevant for optoelectronic applications at ambient temperatures. This study was inspired by the excellent PL properties (especially, the extremely large Stokes shift of the PL, very attractive for sensing purpose and OLEDs) of such a class of DLC compounds and thin films thereof,[33] that have been successfully applied as organic electrical-capacitive sensors for efficient gas-sensing purposes, as recently reported.[34]

Similar to optoelectronic devices based on other semiconductor materials and molecular systems, e.g., the temperature-dependent efficiency of the PV power generation,[35] the thermal effects can influence the PL conversion of TKHD DLC films. Since the photo-induced thermal effects are of primary importance when considering DLCs as PL emitter materials as well as PL-based sensors, we examined the impact of the photothermal effects on the PL stability of TKHD glassy thin films. It was inspected the possibility to stabilize the PL emission from TKHD by means of SWCNTs as nanofillers in this DLC. Along with the refinement of synthesis, purification of DLC molecules, designing novel DLC molecular architectures, and enhancing their thermal stability, the purposeful improvement of PL stability of the DLC luminescent layers is of great importance for the practical implementations of such soft-organic materials.

2. EXPERIMENTAL SECTION

2.1. Materials and Nanocomposite Preparation. The sample preparation was described elsewhere.[31] Briefly, the compound TKHD is a star-shaped DLC. Its molecular structure has a disk-like tris(keto-hydrozone) core with three long branches with six carbon atoms present in each alkoxy tail (Figure 1a). This C_3-symmetric (n,π)-conjugated DLC was synthesized by Yelamaggad and co-workers in the Centre for Nano and Soft Matter Sciences in Bengaluru, India. The molecular structure of TKHD is close to that of the DLC compound abbreviated as HDN5 (five carbon atoms in the peripheral alkoxy tails, instead of six in TKHD) from a DLC series synthesized and investigated by the same research group.[34] The phase transition temperatures of TKHD DLC are given in Table S1 in the Supporting Information.

The SWCNTs EC1.5-P eDIPs were purchased from Meijo Nano Carbon Co., Ltd. Japan and were used as received without any further chemical treatment. The SWCNTs have carbon purity degree higher than 99%. According to the producer's specification, the mean diameter and average length of the SWCNTs were d_{SWCNT} = 1.5 ± 0.5 nm and L_{SWCNT} = 7 μm, respectively. The SWCNTs were a mixture of about 2/3 semiconducting (*s*-SWCNTs) and 1/3 metallic (*m*-SWCNTs).

https://doi.org/10.1021/acsomega.3c02103
ACS Omega 2023, 8, 27102−27116

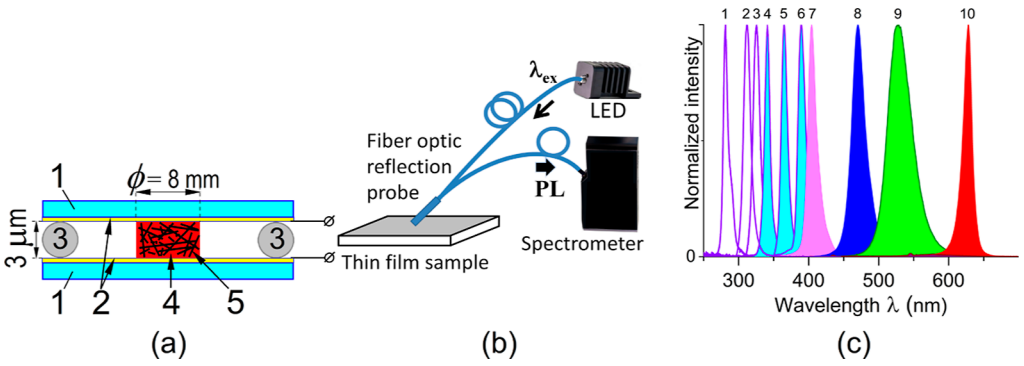

Figure 2. (a) Schematic of a cell with the SWCNT/TKHD NC film for electrical measurements: 1—glass plates; 2—plane cover layers of ITO; 3—spacers; 4—TKHDLC (in red color); 5—CNTs (in black color). The dimensions are not to scale. (b) Schematic of the experimental setup for PL measurement. (c) Emission spectra of the LEDs used in this work. The numbers 1−10 correspond to the LED numbers in Table S2 in the Supporting Information.

SWCNT/TKHD NC was produced by mixing of dispersions of TKHD and SWCNTs. The preparation procedure is schematically shown in Figure 1b. As a solvent for both TKHDLC and SWCNTs was used 1-methyl-2-pyrrolidinone (NMP) (anhydrous a.r.) with purity >99% (from Chem-Lab NV, Zedelgem, Belgium), without any additional purification. Homogeneous dispersions of SWCNTs in NMP (concentration 30 μg/mL) and TKHD (concentration 1 mg/mL) in NMP were obtained at ambient temperature by use of ultrasonic mixer-homogenizer DW-SD20-1200 (Hangzhou Dowell Ultrasonic Technology Co., Ltd, Hangzhou, Zhejiang, China) and ultrasonic processor UP100H (Hielscher Ultrasonics GmbH, Teltow, Germany), respectively. Then, both dispersions were gently mixed and homogenized by ultrasonication. The amounts of both components, the SWCNTs and TKHD, were determined in such a way that the weight ratio SWCNTs/TKHD in the final uniform dispersion was 1:100. The SWCNT/TKHD NCs formed as thin layered samples were produced by slow evaporation of the solvent NMP from this mixture. This was done onto a flat Petri glass dish in a well-controlled way. Thin layers of neat TKHD were prepared in the same manner, i.e., by evaporation from NMP solution of original TKHD LC molecules.

Thin films with a constant thickness (3 μm) were obtained by sandwiching the SWCNT/TKHD NC between two clean (untreated) plane-parallel glass plates (1 cm × 1 cm) with a thickness of 1 mm, forming a symmetric cell (Figure 2a). The thickness of the films was adjusted by spacers of 3 μm thick Mylar foil and was controlled by measurement with a Coolant IP 65 digital micrometer (Mitutoyo Co., Takatsu-ku, Kawasaki, Kanagawa, Japan). For comparative measurements, reference thin films with the same thickness between identical glass plates were also prepared from pure TKHD. The surface of the TKHD and SWCNT/TKHD films was circular-shaped with an area of about 40 and 50 mm^2, respectively. The electrical measurements of the produced thin films were performed with cells assembled with glass plates having electro-conductive nano-coating (~80 nm-thin) of indium tin oxide (ITO) (from Delta Technologies Ltd., Loveland, CO, USA). They serve as electrodes with a low (<10 Ω/□) sheet resistance.

As a final preparation step, the glass cells with the DLC films were heated up to ~200 °C [a little above the isotropization point of the TKHD LC substance (188 °C)],[31] then kept at that temperature about 10 min, and thereafter cooled down to ambient temperature. So cooled, the DLC undergoes a phase transition from the isotropic to columnar (Col) phase. As evidenced in ref 30, the Col LC phase of TKHD was "frozen" into a thermodynamically stable glassy state. We examined during several months that the obtained glassy Col LC state remains permanent at room temperature. This holds even after heating up to reasonable temperatures and at a reasonable heating rate. Then, the glassy Col LC state again persists down to room temperature.

2.2. Methods. The morphology of the produced films was observed by transmission optical microscopy, with universal polarizing microscope NU-2 (VEB Carl Zeiss JENA). Micrographs were taken by a digital microscope camera (Moticam 5MP). UV−vis−NIR transmittance of the prepared thin films was recorded at room temperature by use of spectrophotometer PerkinElmer-Lambda 1050. The spectra were obtained at normal incidence of the light, over the wavelength range λ = 320−1200 nm, with a spectral resolution of 1 nm. The spectra were corrected for both spectral sensitivity of the apparatus and optical response of the cover glass plates of the films.

The PL spectra of the studied films were measured at room temperature by use of mini-spectrophotometer Ocean Insight QE Pro equipped with an optical fiber reflection probe (Ocean Insight QR200-7-UV−vis Premium, 200 μm core, 2 m length) (Figure 2b). The PL spectra were excited by illumination of the films with non-focused light from light-emitting diodes (LEDs)—the LSM series of Ocean Insight, emitting in the continuous wave (cw) regime. Several cw LEDs emitting in the UV and in the visible spectral range were employed in the experiments (Figure 2c). The central wavelength (λ_C) and the spectral width ($\Delta\lambda$, fwhm) of their emission are given in Table S2 in the Supporting Information. These light sources controlled by smart controller-driver have a high long-term stability of optical power (fluctuations <0.1%). Via optical fiber, the non-polarized light from LED was directed at an angle of 45° to the surface of the sample understudy, fully covering it. The PL cone light was detected in the backward direction through the second branch of the optical fiber reflection probe (Figure 2b). The spectral resolution of the recorded PL spectra was 1 nm. No optical spectral filters were used. In order to avoid the influence of the ambient light, the PL experiments were conducted in the dark. The LEDs' light intensity on the samples was controlled with Thorlabs PM100 power-meter equipped with silicon photodiode power-sensor

https://doi.org/10.1021/acsomega.3c02103
ACS Omega 2023, 8, 27102−27116

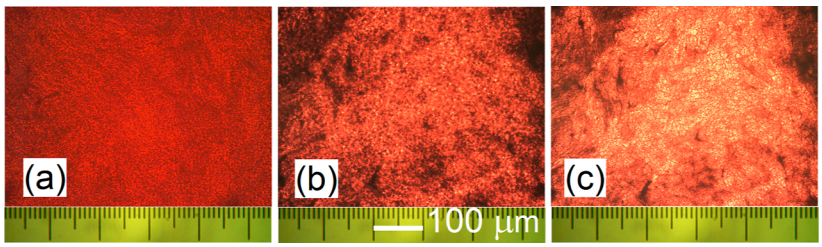

Figure 3. Optical photomicrographs of the textures observed at room temperature (27 °C) for 3 μm thin films of: (a) neat TKHD and (b) SWCNT/TKHD NC. (c) Texture image at the same film location as in (b), but viewed by more intensity of the white light passed through the microscope.

S120VC. In the course of the PL experiments, both excitation and the PL spectra were simultaneously registered, and thus, the value of the excitation optical power was continuously monitored in order its value to be used as a reference.

Frequency spectra of complex electrical impedance of the produced films were obtained at ambient temperature over the range from 1 Hz to 1 MHz of the applied alternating-current (AC) electric field, using impedentiometer workstation BioLogic SP-200 (product of Bio-Logic Science Instruments, Seyssinet-Pariset, Grenoble, France). Electrical impedance spectroscopy (EIS) measurements were carried out at 0.1 and 1 V_{rms} voltage applied between the two electrodes of the cells, for SWCNT/TKHD and TKHD films, respectively. The sine-waveform AC electric field was applied transversally to the film plane. By illumination of the samples with the LEDs, the unfocused light was directed normally to the film plane, the light intensity on the sample was fixed at 1 mW/cm^2. During the measurements, identical experimental conditions were kept, only the exposure dose of the continuous light illumination was varied. The measurements were carried out in normal indoor lighting; the results were practically the same under dark conditions.

A second series of EIS measurements were carried out at the same experimental configurations, but with the variation of the temperature of the films not exposed to light. In this case, the temperature of the films was maintained by thermostat hot stage Mettler FP82 interfaced to a computer. The temperature accuracy was ±0.1 °C. Impedance spectra were recorded one after another in a sequence by interval of 2 °C within the temperature range from 21 to 40 °C. During the series of these measurements by heating of the films, a complementary monitoring of their optical transmittance through the circular glass window of the hot stage was continuously done by use of a spectrophotometer with optical fiber.

3. RESULTS AND DISCUSSION

Because one of the potential applications of the studied TKHD and SWCNT/TKHD thin films is optoelectronics, they were initially characterized by means of optical microscopy and optical spectroscopy.

3.1. Optical Microscopy. At room temperature, the discogen TKHD in the prepared films is in its LC state.[31] Under the optical microscope, the films displayed inhomogeneous morphology—randomly distributed bright and dark micro-domains (Figure 3). The inspection of the optical micrographs indicated that the observed texture can be considered as a hybrid morphology relevant to both LC and glass states. No classical textures typical for ordered and aligned columnar (Col) LC phases having characteristic grainy domains were identified, as well as no textural peculiarities typical for the crystal state of discotics.[9,36] Nevertheless, the TKHD LC texture in Figure 3a resembles the morphology that could be attributed to the disordered Col_r phase.[37,38]

In fact, at room temperatures, the structure of TKHD in the prepared thin films corresponds to a glassy (or glassy-like) Col LC state, as determined by differential scanning calorimetry (DSC).[31] The calorimetric studies have evidenced that when cooled from the isotropic state, the Col phase gets into a glassy state and remains unaltered, as obtained for DLCs having similar molecular structures.[27,33,39−41] Far below the isotropization temperature of TKHD (190 °C), the Col LC phase of this DLC persists, it is not destroyed. By that, the molecular motions of TKHD molecules are strongly hindered. At temperatures in the room-temperature region (20−40 °C), the formed glassy Col LC state is retained. In this permanent state, the disk-like LC molecules of TKHD may form small columnar creatures (by $\pi-\pi$ columnarly stacking of discotic molecules), but not long ordered columns. Thus, when cooled from the isotropic state, a sandy birefringence texture shown in Figure 3a was observed.

More specifically, the morphology of the TKHD films is characterized with smaller textural patterns and is more homogeneous than that of the SWCNT/TKHD NC films. Figure 3a shows structural formations (domains) in the TKHD film that are micrometer-sized and even smaller, with relatively uniform distribution within the viewing scope spatial window. The morphology of SWCNT-filled TKHD becomes more complicated (Figure 3b). At the macroscopic level, these NC films exhibit a cloudy-like and cluster-like microstructure with larger domains and with a broader distribution of domain sizes than those in TKHD films. The sizes of the large domains in SWCNT/TKHD were >10 μm. Also, a fine filament texture in a thread fashion network takes place for these samples (Figure 3b). Clearly, the presence of 1 wt % CNTs produces micro-defects that favor the formation of micro-domains having larger irregular shapes and random orientations. A possible formation of small aggregates of SWCNTs can lead to non-homogeneous dispersion of the SWCNTs in the DLC matrix of the SWCNT/TKHD NC films. This trend would be enhanced when the SWCNT percentage is more. It might be expected that the SWCNT aggregations disturb the molecular ordering (even low) of the host. Furthermore, macro-defects (bubbles, cracks, or others) can also be observed in the volume of the studied glassy films. We should also note that most probably, the SWCNT nanofillers lead to the formation of irregular SWCNT network in the bulk of the SWCNT/TKHD NC films.

Optical microscope images in Figure 3 gave clear evidence of the glassy LC state of the films. The TKHD freezes in a glassy state having a low degree of columnar organization and a low

https://doi.org/10.1021/acsomega.3c02103
ACS Omega 2023, 8, 27102−27116

degree of ordering. This state is fully unorganized, non-ordered (no orientational order, no positional ordering of the formations of disk-like LC molecules). That is why, the adjacent micro-domains have random orientation, and hence, their optical responses are due to random optical phases. The optical images in Figure 3 correspond to diffuse light scattering like that observed by micro-scale heterogeneous, non-uniform, or poly-dispersed LC domain structures reported in literature.[42] The light passing through the studied glassy DLC films undergoes phase modulations by the variety of irregular micro-domains with inhomogeneous spatial distribution and random orientations, thus producing a diffuse light transmittance and scattering.

It should be mentioned that the textures we observed under the microscope did not change upon either the DC (direct current) or AC electric field, applied transversally to the considered films at reasonable voltages. Also, there was no change of the displayed birefringent textures in both TKHD and SWCNT/TKHD glassy films observed by polarizing optical microscopy upon heating of the films from 20 to 40 °C and further up to 60 °C (within this interval, the structure formed in the films remains glassy LC). Furthermore, the same applies to the illumination of the films with cw LEDs emitting in the range from the near UV to the near IR—the observed microscope images of the film structures are the same, regardless of the dose (fluence) of the light.

3.2. Optical Spectroscopy. The studied glassy DLC films were dense and highly opaque and absorbed light very strongly. The color of the TKHD films was red, while the SWCNT/TKHD NC films were of a dark red color. Their optical absorption is in the UV spectral range, as well as in the visible—up to the red (λ ~600 nm) (Figure 4). The wide

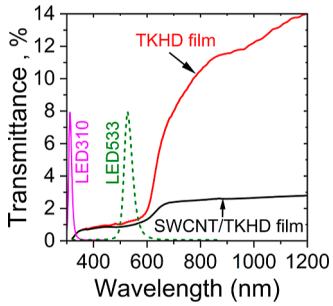

Figure 4. Measured transmission spectra of 3 μm-thick films of TKHD and TKHD filled with SWCNTs. The spectra were recorded under identical experimental conditions at 27 °C. The emission spectra of two of the employed LEDs (λ_C = 312 nm and λ_C = 528 nm) are traced.

absorption spectrum results from convolution of the shapes of two broad spectral bands corresponding to the $\pi-\pi^*$ and $n-\pi^*$ electronic transitions in the molecular system of TKHD. The absorption throughout the visible spectral range makes the compound TKHD a potential candidate for various light-triggered device applications and solar absorber. At wavelengths λ > 600 nm, the transparency of the films is steeply increasing. The filling of TKHD with 1 wt % SWCNTs does considerably reduce the absolute value of optical transmittance, but does not affect the transmittance cut-off spectral shape. Clearly, besides the enhanced optical absorption, the light scattering due to SWCNTs largely contributes to the reduced transmittance of SWCNT/TKHD films. The high absorption of the studied thin films is essential, because this can lead to photo-induced change of their properties and key characteristics.

3.3. Additional Inspection. Additional thermo-optical measurements (transmitted light intensity versus the temperature of the films) were performed by use of a non-focused probe beam of thermo-stabilized He−Ne laser (λ = 632.8 nm) and a highly sensitive photodiode. First, the intensity of the incident probe beam on the sample was kept fixed at 0.1 W/cm^2. By these measurements, we observed that the probe beam intensity transmitted through the studied glassy films was not affected by varying their temperature in the range 20−60 °C. Second, no laser-induced changes of the light transmittance coefficient of the films were registered by varying the He−Ne laser beam intensity up to 10 mW/cm^2 on the sample. Both results were in accordance with the observations with optical microscopy and confirm the lack of structural changes (reversible or irreversible) in the TKHD and SWCNT/TKHD films by such variations of the experimental conditions.

Being important for practical applications, the stability of the studied discotic materials was also estimated. Periodic tests with DSC have shown a fairly good reproducibility of thermograms of both TKHD DLCs and their NCs with SWCNTs studied here. During a test period of more than 1 year, the DSC data from scans in the range 20−100 °C were the same, when the experimental conditions were kept the same.

Because the study presented here concerns mainly the photoresponse of our glassy discotic films upon their temperature variation in the range 25−40 °C, a supplementary verification of the photostability (photochemical stability under irradiation conditions considered here) of the films as well as their long-term stability at temperatures in that range, was also done. They were checked with EIS. In tests over a long time (one year), the EIS data were the same under the same experimental conditions. Also, for such a long period of time, no noticeable change in the properties and quality of the investigated glassy discotic films was observed. In general, at ambient conditions, they exhibit high photostability (tested by means of the resultant PL) and long-term stability (which could be affected by the possible aging of the material), both very important from an application point of view.

Finally, our supplementary measurements by thermogravimetry indicated that the decomposition temperature of the studied glassy-state discotics (TKHD and SWCNT/THKD NC) is ca. 200 °C. Thermogravimetric graphs obtained for our samples (Figure S1, in Supporting Information) reveal similar thermal stability for them. One can consider that the thermal decomposition process for both materials starts at temperatures about 100 °C and becomes intensive above 200 °C. The effect from the nanofiller was evident—the thermal stability of the SWCNT/THKD NC was a little higher. In any case, this is due to the extremely high thermal stability of SWCNTs that is much above 1000 °C.[43] The thermal stability of TKHD is closely related to the chemical stability of this DLC and can be correlated with the structural phase transformation evolution of TKHD during heating (Table S1, in Supporting Information).

The high thermal stability is a fundamental requirement for device applications. The thermograms in Figure S1 show that the adaptability, without any negative impact, and the operation of the considered glassy discotic films is possible at ambient temperature and in a temperature range of working

https://doi.org/10.1021/acsomega.3c02103
ACS Omega 2023, 8, 27102−27116

temperatures preferably up to 100 °C, and not feasible to use in larger temperature range and under extreme conditions. The shift of the weight loss curve corresponding to the NC of SWCNT/TKHDLC, noticed toward a higher temperature, could be indicative of significant interfacial interactions between SWCNTs and TKHDDLC. This contributes to increasing the thermal stability of the SWCNT/TKHD NC.

3.4. Photoluminescence. Figure 5a presents PL spectra of glassy TKHD film, as excited with LEDs whose emission is in the near UV range. The PL appears as a featureless broad band in the red-to-near IR spectral range. The PL spectral band with FWHM of 137 nm was centered at ca. 700 nm. The spectral shape of PL was the same, regardless of the excitation wavelength λ_{ex} in the range from 280 to 470 nm. It is noteworthy that the large Stokes shift of the PL. It can be from ~300 nm (at λ_{ex} = 405 nm) up to ~420 nm (at λ_{ex} = 280 nm). By excitation at λ_{ex} = 528 nm, a well distinguished PL was still registered, although the PL spectrum is very close to the excitation wavelength (Figure 5b).

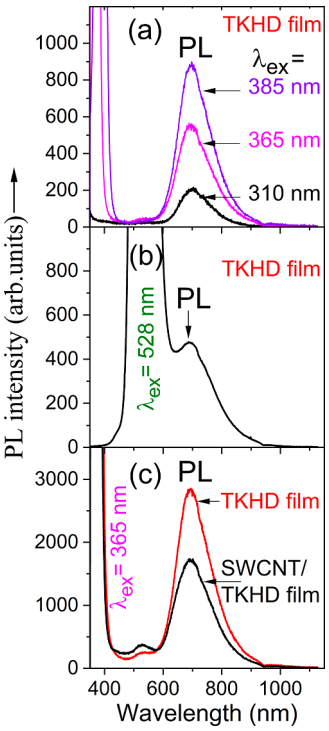

Figure 5. (a,b) PL spectra of TKHD film recorded at various excitation wavelengths; the other experimental conditions were kept the same. (c) Comparison of PL spectra (λ_{ex} = 365 nm) of films of pure TKHD and SWCNT/TKHD NC under identical experimental conditions. The small PL band around 530 nm is due to the glass slides of the film.

As emphasized in ref 33, the large Stokes shift is very scarce for DLCs. Such NIR emission is useful for optic, optoelectronic, photonic, and sensoric applications, e.g., for NIR OLEDs and bioimaging. In our case, the LC columnar mesophase frozen in a glassy state facilitates the high wavelength of the maximum of the PL emission. Compared to the luminescence from solution-state TKHD samples, the PL from the studied TKHD in a glassy thin-film state were red-shifted, as reported and explained for similarly structured DLC compounds.[27,39−41] This valuable property, along with the significantly enhanced PL emission from a frozen Col phase,[33,44] is promising in optoelectronic applications, such as OLEDs. It should be noted that the doping of TKHDLC with 1 wt % SWCNTs did not change the PL bandshape (Figure 5c), but resulted in about a two times lower PL intensity (at identical experimental conditions, as measured at the same geometry configuration and within the same spatial angle of the PL emissions).

The studied TKHD films showed a relatively low efficiency of PL (the ratio of the measured PL intensity to the intensity of the incident light). Moreover, the PL intensity was lower than the intensity of the light at λ_{ex} diffusely reflected and scattered from the studied discotic films. For example, in the geometry shown in Figure 2b for PL registration, the probe signal measured at a given angle of 45° to the film plane, by excitation at λ_{ex} = 385 nm contains a diffuse reflected and scattered light portion whose total intensity was approximately seven times higher than the integral intensity of the excited PL emission (Figure S2, Supporting Information). An attempt to measure the PL quantum yield (Q_{PL}) of the DLC films under study with an integrating sphere (PerkinElmer FL8500) did not give a result. Thus, their PL quantum yield could be estimated to be below 1%, i.e., considerably lower compared to the Q_{PL} > 10% reported for specially deposited and oriented DLC emitters (plane films) designed for OLEDs.[16b,f] It should be noted that the PL quantum yield for these DLC PL materials and systems depends on many factors such as the structural order, molecular orientation, intermolecular and substrate interactions, as well as on all possible energy loses, including a part of the excitation energy dissipated into heat.

The PL stability is a crucial requirement for PL-based sensors, optoelectronic, and other devices. In this regard, a negative effect was observed by our experiments with PL from TKHD thin films exposed to cw light. During continuous illumination, a slight gradual reduction of the PL intensity (entire PL band) occurs until the PL reaches its stationary state (Figure 6). The rate of this light-induced effect depends

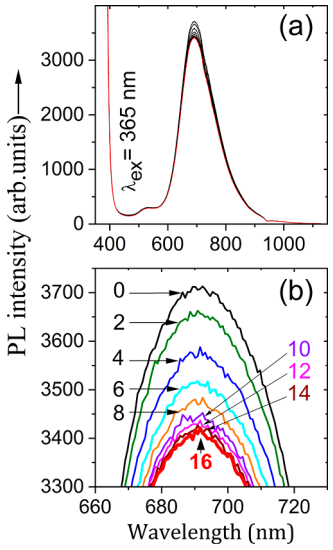

Figure 6. In-time evolution of PL by TKHD film upon continuous illumination at λ_{ex} = 365 nm. The light intensity was fixed at 1 mW/cm^2. The PL spectra (single scans with a spectrophotometer) were recorded under identical experimental conditions. The graph (b) is an enlarged view of the PL peak presented in (a). The numbers denoted in (b) indicate the duration of illumination (in minutes).

https://doi.org/10.1021/acsomega.3c02103
ACS Omega 2023, 8, 27102−27116

on the light fluence—the higher the light fluence, the faster and larger the PL reduction. For instance, at 1 mW/cm^2 (λ_{ex} = 365 nm), the PL from the studied TKHD thin films reaches the steady state (about 10% reduction of intensity) within 14 min, whereas at 5 mW/cm^2, this happens during 8 min.

The observed light-induced effect was reproducible and reversible—when the light was removed, then waited for a certain time, and turned on again, it was found that the PL intensity (the total PL spectrum) tended to return to the initially registered one. By that, the velocity of recovery depends on the cooling of the film (more precisely—it depends on the cooling rate). Since our optical microscopy study showed no macro- and microscopic structural changes in the glassy TKHD films during and after their illumination (see Section 3.1), a reasonable assumption was the photothermal nature of the observed reversible photo-induced effect.

Most likely, the PL reduction is due to thermally activated processes, including thermally activated radiationless processes in the TKHD molecular system by increasing temperature, as suggested for similar luminescent DLC molecular structures.[27,39] In this case, the PL steady state should be relevant to the equilibrium thermodynamical state of the TKHD film, i.e., it depends on thermal conduction and heat transfer in the thin film. Basically, from a photo-chemist's point of view, the luminescence by DLCs involves more than one phenomenon. Furthermore, it should be mentioned that the exact mechanism of competition between the pathways of the various possible photo-induced chemical processes in these molecular systems is not yet completely known.

Significantly, for the thin films of SWCNT/TKHD NC examined here, we have not observed such a negative effect of PL reduction. In order to clarify this difference, we performed EIS investigation on TKHD and SWCNT/TKHD films.

3.5. Photo- and Thermo-Electrical Response of TKHD and SWCNT/TKHD Glassy Films, as Probed by EIS.

3.5.1. TKHD Glassy Films. Figure 7a,b reports the frequency spectra of real (ReZ) and imaginary (ImZ) parts of complex electrical impedance $Z = ReZ + i\,ImZ$ measured for a film of TKHD continuously exposed to UV light. The couples {ReZ, ImZ} were recorded at ambient temperature as a function of the frequency f of the AC electric field applied to the film, upon UV light at increasing dose of the light exposition. The illumination leads to only a little change in ReZ impedance, evident in the low-frequency region of the spectra (below 10 Hz) (Figure 7c). Under the conditions of our experiment, the light does practically not change the ImZ spectrum, i.e., the capacitance of the TKHD films measured between the ITO-glass electrodes remains the same.

It is seen from Figure 7c that the increase (actually, relatively small) of ReZ values toward lower frequencies is enhanced upon UV light. When the light is turned-off, ReZ impedance was found to slowly return to the initial values. We have to point out that there was no change in the ReZ spectra during the time when the film was not illuminated. Furthermore, it should be mentioned that eventual photo-induced structural modifications, degradations or damages in the studied DLC sample at a nano-level (since the UV light could disrupt certain chemical bonds in TKHDLC), can be excluded due to the low illumination intensity, and more importantly—since the observed photoresponse of the TKHD glassy thin film was reversible.

The observed increase in ReZ toward the zero frequency (Figure 7c) seems to be a result of an interfacial effect at the

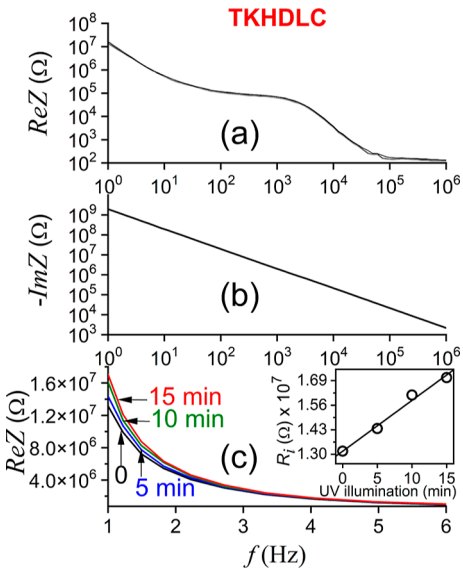

Figure 7. Frequency spectra of real (ReZ) (a) and imaginary (ImZ) (b) parts of complex electrical impedance of TKHDLC film exposed on cw UV light (λ_C = 310 nm); (c)—expanded view of (a) in the low-frequency region. The duration of illumination is given in minutes; 0 means no light. The UV light intensity was 1 mW/cm^2, the temperature of the film at the moment 0 was 27 °C. The insert: the interfacial electrical resistance R_i (at f = 1 Hz) of TKHDLC film vs the dose of the cw UV light. The line represents the corresponding linear fit to the data.

ITO electrode−TKHDLC interface: the electrode polarization (EP) and the corresponding growth of resistive layer at this interface in our symmetric cells can be characterized with the interfacial resistance R_i. EP is an accumulation of long-distance traveled electric charges at the interfaces between the electrode and the dielectric, in our case TKHDLC. At low frequencies, this process dominates over the other dielectric polarization processes. The impact of UV light on R_i of the studied cells with the TKHDLC dielectric in plane-capacitor-like geometry is clear in Figure 7c (the insert therein)—gradually increased values of R_i take place at gradually increasing dose of illumination. From the R_i vs light dose dependence, one can estimate the value 270 kΩ (min mW cm^{-2})$^{-1}$ relevant to the rate of the photo-induced growth of the resistive layer at the electrode−TKHDLC interface due to the processes of diffusion of electric charge carriers.

The photo-induced change in ReZ impedance of TKHD film might be ascribed to photo-induced generation of electric charge carriers or photo-induced electric charge carrier mobility in this DLC, like in other DLCs—organic semiconductors. The photoconductivity of mesophases of DLCs in which the charge carriers are holes or electrons is well known phenomenon.[45] Upon continuous illumination, the photoconductivity of an organic semiconductor placed between two conducting plates—electrodes with an applied voltage—can enhance the EP effect caused by accumulation of photogenerated mobile charge carriers. Note that no other photo-induced changes of Z can be seen in Figure 7, e.g., no appreciable decrease in the ReZ values at higher frequency, in spectral regions beyond the low-frequency region. Such a change would be expected from an effect of photo-induced conductivity associated with generation of photo-current in DLCs.[14,45−50] In this regard, one has to take into account that the direct photoconduction process (contribution of photo-

https://doi.org/10.1021/acsomega.3c02103
ACS Omega 2023, 8, 27102−27116

excited electrons or holes to the electrical transport properties) is most effective by the aligned and highly ordered DLC columnar phase, which is not our case.

Another reasonable hypothesis could be that the considered photo-induced change in *ReZ* spectra of the measured TKHD film is due to a photothermal effect. In this case, the local heating due to light absorption of the film could be the primary effect resulting in a change of *ReZ*. Indeed, by increasing temperature of the same film of TKHDLC but not illuminated, we observed an increase of *ReZ* in nearly the same manner as by UV light (Figure 8). In general, the increase of resistance at

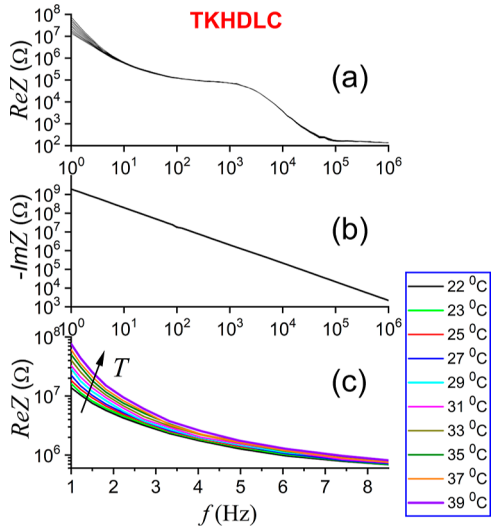

Figure 8. Variation of *ReZ* (a) and *ImZ* (b) spectra of TKHD film with temperature of the film (no UV light); (c) expanded view of (a) in the low-frequency region.

elevating temperature contradicts data from thermoelectric studies reported for DLCs, in particular, in the room-temperature region.[49,51,52] Actually, the possible photothermal effect in TKHD film could be associated with some relatively slow process of generation of electric charge carriers as a secondary process. Thus, the experimental results in Figure 8a can be explained with enhanced EP effect, like for the photo-induced change in *ReZ* spectra (Figure 7c).

In our view, a photothermal process due to the light absorption in the studied film of TKHDLC occurs as an intermediate step, i.e., a photothermoelectrical effect (PTEE) takes place—the photoresponse of the TKHD film is driven by a thermal mechanism, rather than by direct photoexcitation of electric charge carriers. The latter process is still possible, but its contribution should be relatively low because the observed change of the photoresponse of the TKHD film is opposite to the effect of photo-induced conductivity associated with generation of photo-current (due to photon-induced charge carriers) in DLCs (most intensive in the DLC columnar phase).[14,45,47−49] The accurate elucidation of the main mechanism needs measurements of DC conduction behavior, electrical current polarization decay measurements, thermally stimulated depolarization currents and other temperature-dependent measurements, cyclic voltammetry, chronoamperometry, and/or other techniques for measurements in the time domain, especially time-resolved experiments. For our samples, this requires application of suitable concept and adequate theoretical physical models for analysis of time-dependent interfacial resistance, which is out of the focus and scope of the present study. Note that the nature of the photo-induced electric-charge generation, recombination, transport process, and photocurrent mechanism in DLCs is not jet fully understood.

The changes in *ReZ* spectra by light (Figure 7c) can be correlated with the changes resulting from the heating of the same TKHD thin film, but not illuminated (Figure 8c). Thus, from the impedimetric response of TKHD film for our case of UV illumination, the absorption of UV light for 15 min might be considered equivalent to a temperature increase of ca. 1.5 °C. Accordingly, the rate of the light-produced heating can be determined to be $\zeta = 0.1$ °C (min mW cm^{-2})$^{-1}$. This quantity can be a measure for the photo-induced thermal changes due to accumulated photo-produced heat in the studied TKHD thin film.

3.5.2. SWCNT/TKHD Glassy Films. At the relatively high percentage of 1 wt % of SWCNTs, the SWCNT/TKHD NC is

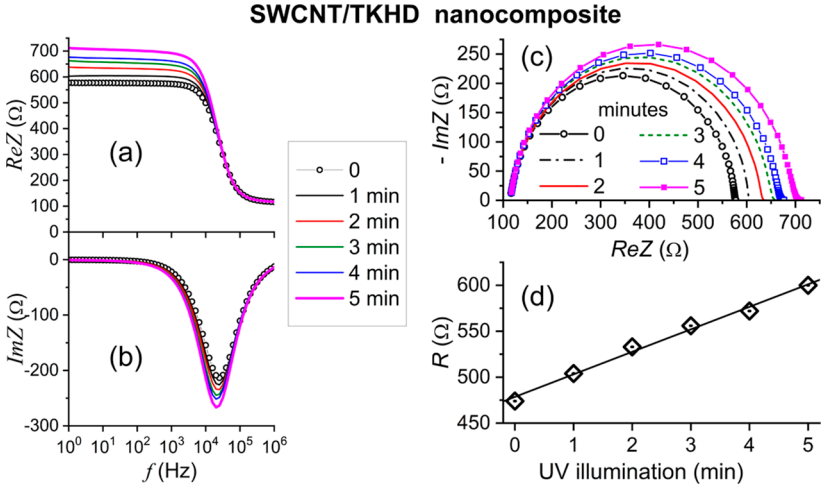

Figure 9. *ReZ* (a) and *ImZ* (b) spectra measured for SWCNT/TKHD film by varying the duration of the illumination of cw UV light (λ_C = 310 nm) (0 means no light). The temperature of the film at the moment 0 was (27 °C), and the UV light intensity was kept fixed at 1 mW/cm^2. The corresponding Nyquist plots are in (c). (d) Electrical resistance *R* of the measured SWCNT/TKHD film vs the dose of the impinging cw UV light, as well as the corresponding linear fit to the data.

https://doi.org/10.1021/acsomega.3c02103
ACS Omega 2023, 8, 27102−27116

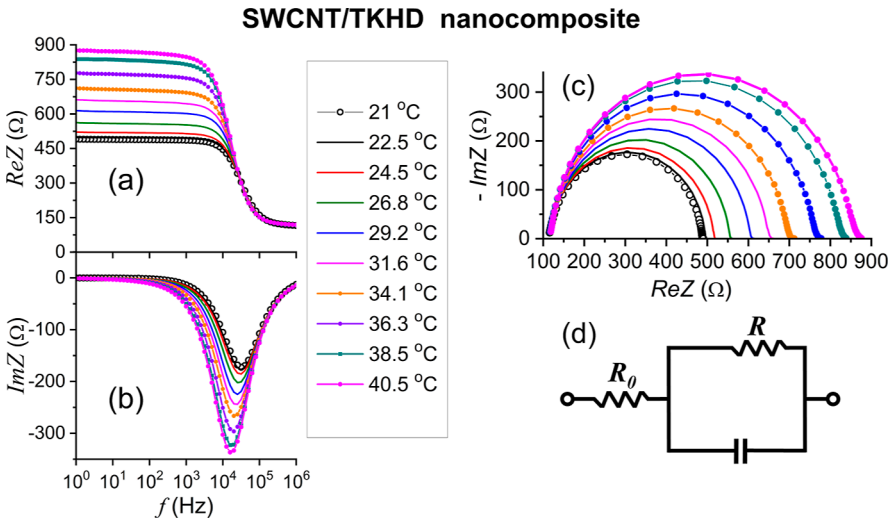

Figure 10. *ReZ* (a) and *ImZ* (b) spectra measured for SWCNTs/TKHD film by varying the temperature of the film (no UV light). The corresponding Nyquist plots (c) and the equivalent electric circuit (d).

highly conductive. As is known, because of their structure of mesoscopic 1D systems, the electronic transport properties of SWCNTs are controlled by quantum size and charging effects, and they possess high electrical conductivities (10^4–10^6 S cm^{-1}).[53] It has to be noted that a formation of a network of randomly dispersed SWCNTs and their aggregates in the prepared films of SWCNT/TKHD NC is rather possible at 1 wt % SWCNT nanoadditives.[54] In our case, the high aspect ratio of SWCNTs ($L_{SWCNT}/d_{SWCNT} > 4000$) is favorable for the formation of network of such carbon nanostructures. Therefore, such a possible assembly should also be taken into account. Regarding the geometric configuration, it should be noted that within the bulk of the SWCNT/TKHD film, a SWCNT network positioned between the contact electrodes most likely connects them in our case (Figure 2a).

Figure 9a,b presents the EIS data obtained for a thin glassy film of SWCNT-filled TKHD when it was continuously illuminated under the same experimental conditions as for the TKHD thin film (see the previous Section 3.5.1), and the {*ReZ*; *ImZ*} spectra were registered every minute. The frequency behaviors of *ImZ* and *ReZ* of SWCNT/TKHD NC look like as those of the highly conductive dielectrics. Toward the zero frequency, the *ReZ* values represent the Ohmic resistance of the sample. Over the whole frequency range covered here, an increase of both *ReZ* and *ImZ* of these films takes place by their illumination. The increase is most pronounced in certain frequency regions—at ca. 10 kHz for *ImZ*, and below 10 kHz for *ReZ*.

Similarly to the studied TKHD films, the observed light-induced change of electrical impedances of the SWCNT/TKHD NC films was reversible—when the illumination is turned-off, the initial impedances of the samples were recovered. The velocity of recovery process was proportional to the rate of the cooling of the films. By our experiments, a clear PTEE in the studied SWCNT/TKHD NC films was also found when they were illuminated with cw LED emitting in the visible (λ_C = 405 nm, λ_C = 470 nm, λ_C = 528 nm, or λ_C = 628 nm). Qualitatively, under identical experimental conditions, the degree of the photothermal effect follows the absorption strength of the films at the corresponding wavelengths (recall Figure 4).

Figure 10a,b shows the temperature-dependent variation of *ReZ* and *ImZ* spectra of the same SWCNT/TKHD film. The comparison with Figure 9a,b strongly suggests that the photoelectrical effect is realized via intermediate photothermal effect, i.e., the absorbed energy increases the temperature of the film, which is observed as a photoresponse due to the temperature dependence of the electrical impedance. By that, the increase of the resistive value of SWCNT/TKHD NC with the increase of the temperature indicates that the semiconductor behavior of the NC impedance cannot be associated to the thermal activation of charge carriers.

The Nyquist complex diagrams (the plots of $-ImZ$ vs *ReZ*) corresponding to the recorded EIS data for the measured SWCNT/TKHD film demonstrated single semi-circular responses (Figures 9c and 10c). In the low-frequency region of the Nyquist plots (the region of the increasing values of *ReZ*), there was no inclined spike relevant to EP. Such a semicircular shape corresponds to the electric circuit of resistance (R) and capacitance connected in parallel (Figure 10d). In the present case, the increase in the *ImZ* peak simply reflects the increase of R. At values of R in the range 470–600 Ω, the position of the *ImZ* peak at ca. 25 kHz corresponds to a capacitance value of about 15 nF. The phenomena that occur at high frequencies (higher than the MHz range) are associated with an "apparent offset" resistance (R_0) (Figure 10c), in our case of ca. 100 Ω. This "initial" resistance is serial and is connected also in series to the electrode. Upon light, or at elevating temperature, the semicircle and its interception with the *ReZ*-axis move toward the higher values of *ReZ*, i.e., the resistance ($R_0 + R$) of the sample is increased. Significantly, no impedance semicircle (or quasi semicircle) response takes place by the reference films of pure TKHD upon light or temperature exposure at the same experimental conditions (Section 3.5.1).

From Figure 9d, one can calculate the value 25 Ω (mW cm^{-2} $min)^{-1}$ for the light-induced increment of the resistance R of the studied SWCNT/TKHD film. Comparing the Nyquist plots in Figures 9c and 10c, one can assess the temperature range in which the light-induced changes of Z of the SWCNTs/TKHD film correspond to the thermo-induced changes of Z of the same film, but not illuminated. Thus, the light-induced changes discussed above correspond to a heating

https://doi.org/10.1021/acsomega.3c02103
ACS Omega 2023, 8, 27102–27116

of the film from 27 to 34 °C (±0.1 °C). The heating rate in this case was estimated to be ζ = 1.4 °C (min mW cm^{-2})$^{-1}$, i.e., 14 times higher than for the TKHD film at the same experimental conditions.

The decrease in electrical conductivity of the studied NC films with elevating temperature or upon lightning was also established by voltammetry studies under DC electric field.[30] Clearly, both photo-electrical and thermo-electrical responses of the SWCNT-filled TKHD glassy films are predominantly due the added nanofillers, but some contribution from the host TKHD is not excluded.

The role of the SWCNT nanofillers in the nanostructured host TKHDLC for the heating and thermally induced processes due to the absorbed optical energy is diverse. First, the SWCNTs contribute to the enhanced light absorption of the SWCNT/TKHD NC (recall Figure 4) through their extremely high absorption coefficient. Second, the well-known photothermal effect by SWCNT structures (either individual SWCNTs or SWCNT networks) (e.g., ref 55) can strongly contribute to the heating of SWCNT/TKHD NC film. It should be noted, however, that the photothermoelectric/bolometric effect was found in thin films of SWCNT structures (e.g, by suspended SWCNT films[56]); their electrical resistance was found to decrease with the light irradiation, i.e., a behavior opposite to the one observed here. The latter differs also from the signal from direct photoconductivity (contribution of photoexcited electrons and holes) from SWCNT themselves, i.e., the case when a photo-current is generated.[57] Third, through their extremely high thermal conductivity (e.g., refs 58−62), the SWCNTs and their network make an efficient heat transfer possible. The latter can be facilitated by eventual coupling between the DLC and the SWCNTs, most probably due to interfacial interaction and $\pi-\pi$ attraction between their aromatic rings. Application of special experimental techniques and more complex analyses and sophisticated interpretation are necessary to evidence and exactly specify the interaction between the LC and the nanofillers at the nano-level, which is beyond the scope of the present work. Thus, the SWCNTs in the SWCNT/TKHD NC films may play a role of thermal nano-transducers that can transfer the heat to the molecules of TKHDLC. Clearly, this can lead to a change of physical properties of the host TKHDLC. Contrariwise, SWCNTs can accept the heat from the TKHD molecules. In this case, figuratively speaking, the SWCNTs can act as cooling nano-radiators within the SWCNT/TKHD NC material. It is also realistic that the heating and the heat dissipation processes in SWCNTs/TKHD occur solely through the SWCNT component of this NC, thereby also avoiding the heating of the DLC host. A further elucidation of the role of SWCNTs and mechanism of PTEE by the studied NC glassy thin films can be gained from analysis of temperature dependence of their resistance.

3.6. Temperature Coefficient of Electrical Resistance of SWCNT/TKHD Glassy Thin Films. Figure 11a depicts the temperature (T) dependence of the resistance (R) of the measured film of SWCNT/TKHD NC, as obtained from data in Figure 10c, as well as the relative change (the increment R/R_{init}), where R_{init} is the resistance of the film at the initial temperature (21 °C), in the course of the measurements. It is seen that in the investigated range of temperature, R is gradually increasing function of T. The mean value $\sigma \sim 10^{-4}$ S/m of the corresponding electrical conductivity calculated for the SWCNT/TKHD NC film at room temperature (Figure 11b) was about 5 orders of magnitude lower than the room-temperature electrical conductivity of s-CNTs and 9−10 orders of magnitude lower than that of the m-CNTs.[63] On the other hand, σ of the SWCNT/TKHD NC film was about 5 orders of magnitude higher than σ of the neat TKHD film. As compared to the individual CNTs, the electrical conductivity of CNT networks is lower, since in them a random sequence of both s-CNTs and m-CNTs does form conduction paths for electrical current. It is well known that junctions between two similar nanotubes (m-CNTs or s-CNTs) have high conductance, and are ohmic, in contrast to the case of two dissimilar nanotubes (m-CNT + s-CNT), where a contact resistance (rectifying $m-s$ Schottky barrier contact) is formed.

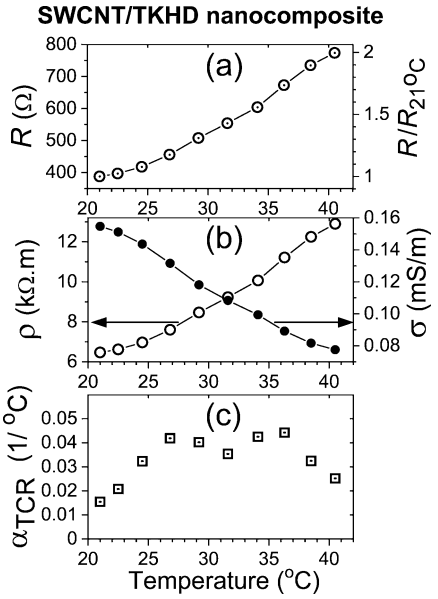

Figure 11. Temperature dependences of the resistance R and its normalized value (a), electrical resistivity ρ and conductivity σ (b), as well as TCR (c), for 3 μm film of SWCNT/TKHD.

From Figure 11a, one can obtain that the temperature derivative of the resistance of the SWCNT/TKHD NC film in the measured range of T, is positive ($dR/dT > 0$). That is, we observed a metallic type of conductivity. This is consistent with the results reported by Dehghani et al.[64] for random networks of SWCNTs containing both m- and s-SWCNTs (in the SWCNT ratio, that is, about 1/3 metallic and 2/3 semiconducting) having dimensions comparable to those of the SWCNTs we employed here. Furthermore, a comparison with the work[64] is reasonable because the cell configuration of the SWCNT/TKHD NC film and the physical conditions in our experiments were very similar to the ones reported in ref 64, in particular, regarding the fact that a part of the SWCNTs in the SWCNT/TKHD film may connect the contact electrodes. In this case, the measured resistance includes three series resistances: (i) the resistance of individual nanotubes; (ii) the resistance between two CNTs crossing each other (the tube−tube resistance), and (iii) nanotube−electrode (ITO) contact resistance.

As is known, the TCR behaviors of individual SWCNTs as well as the SWCNT networks may be different. In general, their R and $R(T)$ should depend on the CNT types, their dimensions, ratio of metallic and semiconducting populations, the levels of defects, configurations, experimental conditions, and other factors. As reported for individual s-SWCNTs with

https://doi.org/10.1021/acsomega.3c02103
ACS Omega 2023, 8, 27102−27116

dimensions comparable to the ones in the present work, their intrinsic electrical resistivity is lowered upon elevating T (in particular, in the considered temperature range 20−40 °C), unlike the individual m-SWCNTs.[64,65] The different thermoelectric behaviors also take place by thin films made of s-SWCNTs or m-SWCNTs, whereas for the mixture of s-SWCNTs or m-SWCNTs, the thermoelectric behavior depends on the compositional ratio of these two types of SWCNTs.[66] As is known, the thermoelectric properties are mostly determined from the semiconductor fraction, whereas the metallic fraction supports a high electrical conductivity.

In contrast to the behavior shown in Figure 11a,b, $R(T)$ in the room-temperature range has been found to be a decreasing function for: (i) self-assembled thin films (2 μm thickness) of a 1:1 mixture of s-SWCNTs and m-SWCNTs;[67] (ii) thin films (12.5 μm-thick) of self-oriented and highly aligned SWCNT in polymer matrix;[68] (iii) thin films (several μm-thick) of suspended networks of SWCNTs;[56,69,70] (iv) inkjet-deposited (printed) SWCNT networks in layers several tens nm-thick;[71] and (v) thin films (10−20 μm) of bulk insulating matrix (e.g., polymer) with dispersed SWCNTs at a small volume fraction (e.g., ranging from 0.1 to 8%),[72,73] where, statistically, the quantity of s-SWCNTs is twice that of the m-SWCNTs. Further, $dR/dT < 0$ was found for intrinsic SWCNT networks with s-SWCNTs >90% (e.g., ref 74) and for pure s-SWCNT networks (e.g., ref 75).

It is well-known that the electrical behavior of SWCNT networks strongly depends on the network density.[76−79] Thin films containing SWCNT network structures at low network densities exhibit $dR/dT < 0$.[76,77] In this case, the conductivity mechanism is different from the one for dense SWCNT networks. On the other hand, a positive dR/dT in the room-temperature region has the single- and few-wall CNT interconnects,[80] as well as the mixed SWCNTs (m-SWCNTs + s-SWCNTs) and their networks.[64,66] Figure 11c shows the values of the temperature coefficient of the resistance (TCR), $\alpha = dR/R\ dT$, for the studied SWCNT/TKHD NC film, as calculated from the $R(T)$ dependence in Figure 11a. The mean value of the calculated TCR at room temperature was α = 0.03/°C, ±0.01/°C. The positive TCR of the SWCNT/TKHD NC film is in contrast to TCR measured for the bolometer-sensitive micrometer-thin films based on mixtures of s-SWCNTs and m-SWCNTs that also exhibit PTEE, but such films are characterized with negative TCR values, in particular, in the room-temperature region.[56,67,68,73,81]

Taken together, all the data and the obtained results discussed above lead us to conclude that it is reasonable to think that the PTEE observed in the studied SWCNT/TKHD NC films is mainly realized through SWCNT networks randomly formed in these films. Although the light is absorbed also from the DLC host, the light-produced heating and the corresponding thermo-induced effects in the volume of SWCNT/TKHD NC films are predominantly due to SWCNTs. The heating in these films is thermally conducted and dissipated by SWCNT network within the films. Due to the huge difference between the thermal conductivities of SWCNTs and TKHD, the heat released in the latter is negligible. Thus, the SWCNT fillers acting as nanoscale coolers prevent the heating of the host TKHD and thereby avoid the light-induced drop of PL intensity that occurs in neat TKHD films (discussed in Section 3.4). Of note, CNTs have long been used for thermal management (heat removal/dissipation) as an efficient heatsink nanomaterial in chip cooling applications (e.g., refs 82−84).

4. CONCLUSIONS

At room temperature and by excitation with light in the UV, as well as in the violet range of the visible, the studied thin films (3 μm) of glassy liquid-crystalline discotics TKHD and TKHD filled with 1 wt % SWCNTs exhibit intensive PL in the deep red with extremely large Stokes shift. Hence, they are promising materials for development of emissive layers in optoelectronic devices. However, upon continuous illumination even at relatively low-intensity (~1 mW/cm^2), the PL response of TKHD thin films has diminished in the time. The nature of this unwanted effect was clarified. The experimental results obtained upon light and thermal exposure of the studied films show that the PL drop is not due to light-induced structural changes in the films, but to a photo-thermal effect. The analysis of the data indicates that the photo-electrical response of the films is caused by a thermal mechanism.

Significantly, the presence of SWCNTs in glassy TKHD LC thin films eliminates the photo-induced decrease of PL from these films, thereby providing a stable PL intensity desirable for optoelectronic application. The highly conductive SWCNT nanofillers and most probably their random network in the SWCNT/TKHD NC films absorb and dissipate the photo-induced heating, thus acting as an effective cooling substructure (nano-scale elements like heat sinks). At the same time, the LC properties of the SWCNT/TKHD NC remain unchanged. Our future investigations will explore the application of the studied conductive NCs of highly photo-responsive tris(keto-hydrozone) DLC for sensing vapors of volatile organic compounds, utilizing the long-wavelength luminescence and the stable operation of corresponding devices, as well as their use for special thin-film photo-controllable detection schemes.

■ ASSOCIATED CONTENT

Supporting Information

The Supporting Information is available free of charge at https://pubs.acs.org/doi/10.1021/acsomega.3c02103.

Phase transition temperatures; optical parameters of LEDs; thermogravimetric graph; and integral area of photoluminescence spectrum (PDF)

■ AUTHOR INFORMATION

Corresponding Author

Georgi B. Hadjichristov − *Laboratory of Optics & Spectroscopy, Georgi Nadjakov Institute of Solid State Physics, Bulgarian Academy of Sciences, Sofia BG-1784, Bulgaria*; orcid.org/0000-0002-7141-3537; Email: georgibh@issp.bas.bg

Author

Yordan G. Marinov − *Laboratory of Liquid Crystals & Biomolecular Layers, Georgi Nadjakov Institute of Solid State Physics, Bulgarian Academy of Sciences, Sofia BG-1784, Bulgaria*

Complete contact information is available at: https://pubs.acs.org/10.1021/acsomega.3c02103

Notes

The authors declare no competing financial interest.

https://doi.org/10.1021/acsomega.3c02103
ACS Omega 2023, 8, 27102−27116

■ ACKNOWLEDGMENTS

We would like to express our sincere thanks to Dr. C. V. Yelamaggad, Dr. S. Krishna Prasad, and Dr. B. N. Veerabhadraswamy from the Centre for Nano and Soft Matter Sciences, Jalahalli—Bengaluru, Karnataka (India), for supplying the discotic liquid crystals. The optical equipment used in this work was funded by the European Regional Development Fund, as a part of the Operational Programme "Science and Education for Smart Growth 2014−2020", Project: CoE "National Center of Mechatronics and Clean Technologies", BG05M2OP001-1.001-0008-C01. The authors are extremely thankful Professor Stoyan Gutzov from Sofia University "St. Kliment Ohridski", Faculty of Chemistry and Pharmacy, for the probe measurements with PerkinElmer FL8500 Integrating Sphere (used with FL 8500 Fluorescence Spectrophotometer). The expert technical assistance from Assist. T. Vlakhov from ISSP-BAS, Bulgaria, is also gratefully acknowledged.

■ REFERENCES

(1) Simpson, C. D.; Wu, J.; Watson, M. D.; Müllen, K. From graphite molecules to columnar superstructures—an exercise in nanoscience. *J. Mater. Chem.* **2004**, *14*, 494−504.

(2) Achalkumar, A. S.; Mathews, M.; Li, Q. Stimuli-directed self-organized one-dimensional organic semiconducting nanostructures for optoelectronic applications. In *Functional Organic and Hybrid Nanostructured Materials: Fabrication, Properties, and Applications*; Li, Q., Ed.; Wiley-VCH Verlag GmbH & Co. KGaA: Weinheim, Germany, 2018; pp 247−306, Chapter 7.

(3) Seguy, I.; Jolinat, P.; Destruel, P.; Farenc, J.; Mamy, R.; Bock, H.; Ip, J.; Nguyen, T. P. J. Red organic light emitting device made from triphenylene hexaester and perylene tetraester. *Appl. Phys.* **2001**, *89*, 5442−5448.

(4) Dong, S.; Tian, H.; Song, D.; Yang, Z.; Yan, D.; Geng, Y.; Wang, F. The first liquid crystalline phthalocyanine derivative capable of edge-on alignment for solution processed organic thin-film transistors. *Chem. Commun.* **2009**, *45*, 3086−3088.

(5) Schmidt-Mende, L.; Fechtenkötter, A.; Müllen, K.; Moons, E.; Friend, R. H.; MacKenzie, J. D. Self-organized discotic liquid crystals for high-efficiency organic photovoltaics. *Science* **2001**, *293*, 1119−1122.

(6) Chandrasekhar, S. Discotic liquid crystals. A brief review. *Liq. Cryst.* **1993**, *14*, 3−14.

(7) Bisoyi, H. K.; Kumar, S. Discotic nematic liquid crystals: science and technology. *Chem. Soc. Rev.* **2010**, *39*, 264−285.

(8) Bushby, R.; Kawata, K. Liquid crystals that affected the world: Discotic liquid crystals. *Liq. Cryst.* **2011**, *38*, 1415−1426.

(9) Kumar, S. *Chemistry of Discotic Liquid Crystals: From Monomers to Polymers*, 1st ed.; CRC Press: Boca Raton, FL, USA, 2011.

(10) Bisoyi, H. K.; Li, Q. Directing self-organized columnar nanostructures of discotic liquid crystals for device applications. In *Nanoscience with Liquid Crystals: From Self-Organized Nanostructures to Applications*; Li, Q., Ed.; *Springer Series in NanoScience and Technology*; Springer: Cham, Switzerland, 2014; pp 209−256. Chapter 7.

(11) Wöhrle, T.; Wurzbach, I.; Kirres, J.; Kostidou, A.; Kapernaum, N.; Litterscheidt, J.; Haenle, J. C.; Staffeld, P.; Baro, A.; Giesselmann, F.; Laschat, S. Discotic liquid crystals. *Chem. Rev.* **2016**, *116*, 1139−1241.

(12) McNeill, A.; Bushby, R. J.; Evans, S. D.; Liu, Q.; Movaghar, B.; Crawley, D. Discotic liquid crystals. In *3D Nanoelectronic Computer Architecture and Implementation*; Nikolic, K., Forshaw, M., Eds.; *Materials Science and Engineering*; IOP Publication Ltd: Bristol, UK, 2005; pp 203−223. Chapter 9.

(13) (a) Sergeyev, S.; Pisula, W.; Geerts, Y. Discotic liquid crystals: a new generation of organic semiconductors. *Chem. Soc. Rev.* **2007**, *36*, 1902−1929. (b) Laschat, S.; Baro, A.; Steinke, N.; Giesselmann, F.; Hägele, C.; Scalia, G.; Judele, R.; Kapatsina, E.; Sauer, S.; Schreivogel, A.; Tosoni, M. Discotic liquid crystals: from tailor-made synthesis to plastic electronics. *Angew. Chem., Int. Ed.* **2007**, *46*, 4832−4887. (c) Kaafarani, B. R. Discotic liquid crystals for opto-electronic applications. *Chem. Mater.* **2011**, *23*, 378−396. (d) Xue, C.; Li, Q. Self-organized semiconducting discotic liquid crystals for optoelectronic applications. *Liquid Crystals Beyond Displays: Chemistry, Physics, and Applications*; Li, Q., Ed.; John Wiley & Sons: Hoboken, NJ, USA, 2012; pp 29−82, Chapter 2. (e) Kumar, S. Functional discotic liquid crystals. *Isr. J. Chem.* **2012**, *52*, 820−829. (f) Shimizu, Y. Discotic liquid crystalline blends for nano-structure formation toward bulk heterojunction active layer in organic photovoltaics. In *Nanoscience with Liquid Crystals: From Self-Organized Nanostructures to Applications*; Li, Q., Ed.; *Springer Series in NanoScience and Technology*; Springer: Cham, Switzerland, 2014; pp 257−280, Chapter 8. (g) Vinayakumara, D. R.; Kumar, M.; Sreekanth, P.; Philip, R.; Kumar, S. Synthesis, characterization and nonlinear optical studies of novel blue-light emitting room temperature truxene discotic liquid crystals. *RSC Adv.* **2015**, *5*, 26596−26603. (h) Gupta, R. K.; Manjuladevi, V.; Karthik, C.; Choudhary, K. Thin films of discotic liquid crystals and their applications. *Liq. Cryst.* **2016**, *43*, 2079−2091. (i) Gülmez, A. D.; Polyakov, M. S.; Volchek, V. V.; Kostakoglu, S. T.; Esenpinar, A. A.; Basova, T. V.; Durmus, M.; Gürek, A. G.; Ahsen, V.; Banimuslem, H. A.; Hassan, A. K. Tetrasubstituted copper phthalocyanines: Correlation between liquid crystalline properties, films alignment and sensing properties. *Sens. Actuators, B* **2017**, *241*, 364−375. (j) Wang, S.; Wang, A.; Yang, C.; Gao, R.; Liu, X.; Chen, J.; Wang, Z.; Zeng, Q.; Liu, X.; Zhou, H.; Zhang, L. Six-arm star polymer based on discotic liquid crystal as high performance all-solid-state polymer electrolyte for lithium-ion batteries. *J. Power Sources* **2018**, *395*, 137−147. (k) Gowda, A.; Jacob, L.; Joy, N.; Philip, R.; Kumar, S. Novel phenazine fused triphenylene discotic liquid crystals: synthesis, characterisation, thermal, optical and nonlinear optical properties. *New J. Chem.* **2018**, *42*, 19034−19042. (l) Bala, I.; Singh, N.; Yadav, R. A. K.; De, J.; Gupta, S. P.; Singh, D. P.; Dubey, D. K.; Jou, J. H.; Douali, R.; Pal, S. K. Room temperature perylene based columnar liquid crystals as solid-state fluorescent emitters in solution-processable organic light-emitting diodes. *J. Mater. Chem. C* **2020**, *8*, 12485−12494. (m) Kumar, S. Investigations on discotic liquid crystals. *Liq. Cryst.* **2020**, *47*, 1195−1203. (n) Chen, H. H.; Cigl, M.; Cheng, C. T.; Bogdanowicz, K. A.; Iwan, A.; Podoliak, N.; Vankátová, P.; Hamplová, V.; Dysz, K.; Przybył, W.; Nitschke, P.; Schab-Balcerzak, E.; Pociecha, D.; Bubnov, A. Self-assembling discotic materials with low symmetry for organic photovoltaics. *J. Mol. Liq.* **2022**, *354*, 118868.

(14) Mathews, M.; Li, Q. Self-organized discotic liquid crystals as novel organic semiconductors. In *Self-Organized Organic Semiconductors: From Materials to Device Applications*, 1st ed.; Li, Q., Ed.; John Wiley & Sons: Hoboken, NJ, USA, 2011; pp 83−129, Chapter 4.

(15) (a) Bushby, R. J.; Tate, D. J. Columnar liquid crystalline semiconductors. In *Liquid Crystalline Semiconductors: Materials, Properties and Applications*; Bushby, R., Kelly, S., O'neill, M., Eds.; *Springer Series in Materials Science*; Springer: Dordrecht, The Netherlands, 2013; pp 65−96. (b) Pisula, W.; Müllen, K. Discotic liquid crystals as organic semiconductors. In *Handbook of Liquid Crystals, Vol. 8 "Applications of Liquid Crystals", Part II: Non-Display Applications and Functions*; Goodby, J. W., Collings, P. J., Kato, T., TschierskeGleeson, H. F., Raynes, P., Eds.; Wiley-VCH Verlag GmbH & Co. KGaA: Weinheim, Germany, 2014; pp 617−674, Chapter 20. (c) Setia, S.; Sidiq, S.; De, J.; Pani, I.; Pal, S. K. Applications of liquid crystals in biosensing and organic light-emitting devices: future aspects. *Liq. Cryst.* **2016**, *43*, 2009−2050. (d) Mu, B.; Hao, X.; Chen, J.; Li, Q.; Zhang, C.; Chen, D. Discotic columnar liquid-crystalline polymer semiconducting materials with high charge-carrier mobility via rational macromolecular engineering. *Polym. Chem.* **2017**, *8*, 3286−3293. (e) Termine, R.; Golemme, A. Charge mobility in discotic liquid crystals. *Int. J. Mol. Sci.* **2021**, *22*, 877.

(16) (a) Vinayakumara, D. R.; Swamynathan, K.; Kumar, S.; Adhikari, A. V. Optoelectronic exploration of novel non-symmetrical

https://doi.org/10.1021/acsomega.3c02103
ACS Omega 2023, 8, 27102−27116

star-shaped discotic liquid crystals based on cyanopyridine. *New J. Chem.* **2018**, *42*, 16999−17008. (b) Keum, C.; Becker, D.; Archer, E.; Bock, H.; Kitzerow, H.; Gather, M. C.; Murawski, C. Organic light-emitting diodes based on a columnar liquid-crystalline perylene emitter. *Adv. Opt. Mater.* **2020**, *8*, 2000414. (c) Jacob, L.; Gowda, A.; Kumar, S.; Belyaev, V. Synthesis, thermal and photophysical studies of π−extended dibenzophenazine based discotic liquid crystals. *J. Mol. Liq.* **2020**, *320*, 114419. (d) Spiess, H. W. Improving organisation of discotics: annealing, shape, side groups, chirality. *Liq. Cryst.* **2020**, *47*, 1880−1885. (e) Vadivel, M.; Singh, S.; Singh, D. P.; Raghunathan, V. A.; Kumar, S. Ambipolar charge transport properties of naphthophenanthridine discotic liquid crystals. *J. Phys. Chem. B* **2021**, *125*, 10364−10372. (f) De, R.; Sharma, S.; Sengupta, S.; Kumar Pal, S. Discs to a "bright" future: exploring discotic liquid crystals in organic light emitting diodes in the era of new-age smart materials. *Chem. Rec.* **2022**, *22*, No. e202200056.

(17) (a) Shoji, Y.; Kobayashi, M.; Kosaka, A.; Haruki, R.; Kumai, R.; Adachi, S.; Kajitani, T.; Fukushima, T. Design of discotic liquid crystal enabling complete switching along with memory of homeotropic and homogeneous alignment over a large area. *Chem. Sci.* **2022**, *13*, 9891−9901. (b) Sivakumar, I.; Swamynathan, K.; Ram, D.; Raghunathan, V. A.; Kumar, S. Rubicene, an unusual contorted core for discotic liquid crystals. *Chem.−Asian J.* **2022**, *17*, No. e202200073. (c) Lin, Y. C.; Li, G. S.; Yu, P. J.; Ercan, E.; Chen, W. C. Organic liquid crystals in optoelectronic device applications: Field-effect transistors, nonvolatile memory, and photovoltaics. *J. Chin. Chem. Soc.* **2022**, *69*, 1289−1304. (d) He, C.; Wang, K.; Wang, Y.; Xu, S.; Liu, Y.; Cao, S. Properties tuning of supramolecular discotics by non-mesogenic triazines and acids. *Aust. J. Chem.* **2022**, *75*, 369−380. (e) De, J.; Sarkar, I.; Yadav, R. A. K.; Bala, I.; Gupta, S. P.; Siddiqui, I.; Jou, J. H.; Pal, S. K. Luminescent columnar discotics as highly efficient emitters in pure deep-blue OLEDs with an external quantum efficiency of 4.7%. *Soft Matter* **2022**, *18*, 4214−4219. (f) Bala, I.; Kaur, H.; Maity, M.; Yadav, R. A. K.; De, J.; Gupta, S. P.; Jou, J.-H.; Pandey, U. K.; Pal, S. K. Electroluminescent aggregation-induced emission-active discotic liquid crystals based on alkoxy cyanostilbene-functionalized benzene-tricarboxamide with ambipolar charge transport. *ACS Appl. Electron. Mater.* **2022**, *4*, 1163−1174. (g) Singh, D. P.; Shah, A.; Bala, I.; Marichandran, V.; Pal, S. K.; Srivastava, A. K.; Kumar, S. Organic electronic applications and charge transport mechanism in novel discotic liquid crystals. *Liq. Cryst.* **2023**, 1−8.

(18) Kumar, S. Nanopraticles in discotic liquid crystals. In *Liquid Crystals With Nano And Microparticles*; Lagerwall, J. P. F., Scalia, G., Eds.; World Scientific Publ.: Singapore, 2017; pp 461−496, Chapter 13.

(19) Gowda, A.; Kumar, S. Recent advances in discotic liquid crystal-assisted nanoparticles. *Materials* **2018**, *11*, 382.

(20) Joshi, A.; Manjuladevi, V.; Gupta, R. K.; Kumar, S. Morphological transformation in the supramolecular assembly of discotic liquid crystal molecules using silver nanoparticles and its sensing application. *Nanotechnology* **2020**, *31*, 365605.

(21) Kumar, M.; Varshney, S.; Kumar, S. Emerging nanoscience with discotic liquid crystals. *Polym. J.* **2021**, *53*, 283−297.

(22) Khare, A.; Uttam, R.; Kumar, S.; Dhar, R. Nanocomposite system of a discotic liquid crystal doped with thiol capped gold nanoparticles. *J. Mol. Liq.* **2022**, *366*, 120215.

(23) (a) Avouris, P.; Radosavljević, M.; Wind, S. J. Carbon nanotube electronics and optoelectronics. In *Applied Physics of Carbon Nanotubes: Fundamentals of Theory, Optics and Transport Devices, Springer Series in NanoScience and Technology*; Rotkin, S. V., Subramoney, S., Eds.; Springer: Berlin, 2005; pp 227−251, Chapter 9. (b) Jagota, A.; Diner, B. A.; Boussaad, S.; Zheng, M. Carbon nanotube-biomolecule interactions: applications in carbon nanotube separation and biosensing. In *Applied Physics of Carbon Nanotubes: Fundamentals of Theory, Optics and Transport Devices, Springer Series in NanoScience and Technology*; Rotkin, S. V., Subramoney, S., Eds.; Springer: Berlin, 2005; pp 253−271, Chapter 10. (c) Jariwala, D.; Sangwan, V. K.; Lauhon, L. J.; Marks, T. J.; Hersam, M. C. Carbon nanomaterials for electronics, optoelectronics, photovoltaics, and sensing. *Chem. Soc. Rev.* **2013**, *42*, 2824−2860. (d) Park, S.; Vosguerichian, M.; Bao, Z. A review of fabrication and applications of carbon nanotube film-based flexible electronics. *Nanoscale* **2013**, *5*, 1727−1752. (e) Cai, L.; Wang, C. Carbon nanotube flexible and stretchable electronics. *Nanoscale Res. Lett.* **2015**, *10*, 320. (f) Zaumseil, J. Single-walled carbon nanotube networks for flexible and printed electronics. *Semicond. Sci. Technol.* **2015**, *30*, 074001. (g) Roman, C. I.; Helbling, T.; Haluška, M.; Hierold, C. Single-walled carbon nanotube sensor concepts. In *Springer Handbook of Nanotechnology, Springer Handbooks*; Bhushan, B., Ed.; Springer: Berlin, 2017; pp 431−456. (h) Oseli, A.; Vesel, A.; Zagar, E.; Perse, L. S. Mechanisms of single-walled carbon nanotube network formation and its configuration in polymer-based nanocomposites. *Macromolecules* **2021**, *54*, 3334−3346. (i) Wei, S.; Zhang, Y.; Lv, H.; Deng, L.; Chen, G. SWCNT network evolution of PEDOT:PSS/SWCNT composites for thermoelectric application. *Chem. Eng. J.* **2022**, *428*, 131137.

(24) (a) Wang, P.; Song, T.; Abo-Dief, H. M.; Song, J.; Alanazi, A. K.; Fan, B.; Huang, M.; Lin, Z.; Altalhi, A. A.; Gao, S.; Yang, L.; Liu, J.; Feng, S.; Cao, T. Effect of carbon nanotubes on the interface evolution and dielectric properties of polylactic acid/ethylene−vinyl acetate copolymer nanocomposites. *Adv. Compos. Hybrid Mater.* **2022**, *5*, 1100−1110. (b) He, Y.; Zhou, M.; Mahmoud, M. H. H.; Lu, X.; He, G.; Zhang, L.; Huang, M.; Elnaggar, A. Y.; Lei, Q.; Liu, H.; Liu, C.; Azab, I. H. E. Multifunctional wearable strain/pressure sensor based on conductive carbon nanotubes/silk nonwoven fabric with high durability and low detection limit. *Adv. Compos. Hybrid Mater.* **2022**, *5*, 1939−1950. (c) Yan, Z.; Wang, S.; Bi, J.; He, Q.; Song, H.; El Azab, I. H.; El-Bahy, S. M.; Elnaggar, A. Y.; Huang, M.; Mahmoud, M. H. H.; Wang, J.; Shao, Q. Strengthening waterborne acrylic resin modified with trimethylolpropane triacrylate and compositing with carbon nanotubes for enhanced anticorrosion. *Adv. Compos. Hybrid Mater.* **2022**, *5*, 2116−2130. (d) Liu, M.; Wu, H.; Wu, Y.; Xie, P.; Pashameah, R. A.; Abo-Dief, H. M.; El-Bahy, S. M.; Wei, Y.; Li, G.; Li, W.; Liang, G.; Liu, C.; Sun, K.; Fan, R. The weakly negative permittivity with low-frequency-dispersion behavior in percolative carbon nanotubes/epoxy nanocomposites at radio-frequency range. *Adv. Compos. Hybrid Mater.* **2022**, *5*, 2021−2030. (e) Tian, T.; Cheng, Y.; Sun, Z.; Huang, K.; Lei, M.; Tang, H. Carbon nanotubes supported oxygen reduction reaction catalysts: role of inner tubes. *Adv. Compos. Hybrid Mater.* **2023**, *6*, 7.

(25) (a) Wang, X.; Wang, H.; Liu, B. Carbon nanotube-based organic thermoelectric materials for energy harvesting. *Polymers* **2018**, *10*, 1196. (b) Hung, N. T.; Nugraha, A. R. T.; Saito, R. Thermoelectric properties of carbon nanotubes. *Energies* **2019**, *12*, 4561. (c) Hayashi, D.; Nakai, Y.; Kyakuno, H.; Hongo, N.; Miyata, Y.; Yanagi, K.; Maniwa, Y. Thermoelectric properties of single-wall carbon nanotube networks. *Jpn. J. Appl. Phys.* **2019**, *58*, 075003. (d) Yang, X.; Cui, J.; Xue, K.; Fu, Y.; Li, H.; Yang, H. Thermal conductivity and thermoelectric properties in 3D macroscopic pure carbon nanotube materials. *Nanotechnol. Rev.* **2021**, *10*, 178−186. (e) Dash, A.; Scheunemann, D.; Kemerink, M. Comprehensive model for the thermoelectric properties of two-dimensional carbon nanotube networks. *Phys. Rev. Appl.* **2022**, *18*, 064022.

(26) Li, X.; Yu, Z.; Zhou, H.; Yang, F.; Zhong, F.; Mao, X.; Li, B.; Xin, H.; Gao, C.; Wang, L. Promoting the thermoelectric performance of single-walled carbon nanotubes by inserting discotic liquid-crystal molecules. *ACS Sustainable Chem. Eng.* **2021**, *9*, 1891−1898.

(27) Yelamaggad, C. V.; Achalkumar, A. S.; Rao, D. S. S.; Prasad, S. K. Luminescent liquid crystalline tris(*N*-salicylideneaniline)s: synthesis and characterization. *J. Org. Chem.* **2009**, *74*, 3168−3171.

(28) Lehman, M. Star-shaped mesogenes − hekates: The most basic star structure with three branches. In *Liquid Crystals: Materials Design and Self-Assembly*; Tschierske, C., Ed.; *Topics in Current Chemistry*; Springer-Verlag: Berlin, 2012; Vol. *318*, pp 193−223.

(29) (a) Detert, H. Tristriazolotriazines: luminescent discotic liquid crystals. *Eur. J. Org. Chem.* **2018**, *2018*, 4501−4507. (b) Tober, N.; Rieth, T.; Lehmann, M.; Detert, H. Synthesis, thermal, and optical properties of tris(5-aryl-1,3,4-oxadiazol-2-yl)-1,3,5-triazines, new star-shaped fluorescent discotic liquid crystals. *Chem.—Eur. J.* **2019**, *25*,

https://doi.org/10.1021/acsomega.3c02103
ACS Omega 2023, 8, 27102−27116

15295−15304. (c) Tober, N.; Winter, J.; Jochem, M.; Lehmann, M.; Detert, H. Tris(5-aryl-1,3,4-oxadiazolyl)benzotrithiophenes—discotic liquid crystals with enormous mesophase ranges. *Eur. J. Org. Chem.* **2021**, *2021*, 798−809.
(30) Hadjichristov, G. B.; Exner, G. K.; Marinov, Y. G.; Vlakhov, T. E. Photo-electrical response of nanocomposites from single-walled carbon nanotubes incorporated in tris(keto-hydrozone) discotic mesogen. *J. Phys.: Conf. Ser.* **2021**, *1762*, 012011.
(31) Exner, G. K.; Marinov, Y. G.; Hadjichristov, G. B. Novel nanocomposites of single wall carbon nanotubes and discotic mesogen with tris(keto-hydrozone) core. *C. R. Acad. Bulg. Sci.* **2020**, *73*, 1217−1224.
(32) Chen, H. M. P.; Ou, J. J.; Chen, S. H. Glassy liquid crystals as self-organized films for robust optoelectronic devices. In *Nanoscience with Liquid Crystals: From Self-Organized Nanostructures to Applications*; Li, Q., Ed.; *NanoScience and Technology Book Series*; Springer International Publishing: Cham, Switzerland, 2014; pp 179−208, Chapter 6.
(33) Nayak, R. A.; Veerabhadraswamy, B. N.; Shankar Rao, D. S.; Sudhakar, A. A.; Yelamaggad, C. V. Room-temperature, deep-red/NIR-Emissive, C_3-symmetric (n,π-conjugated) columnar liquid crystals: C_{3h}-tris(keto-hydrazone)s. *ACS Omega* **2021**, *6*, 3291−3306.
(34) Yuvaraja, S.; Bhyranalyar, V. N.; Bhat, S. A.; Vijjapu, M. T.; Surya, S. G.; Yelamaggad, C. V.; Salama, K. N. Tris(keto-hydrazone): a fully integrated highly stable and exceptionally sensitive H_2S capacitive sensor. *Adv. Electron. Mater.* **2021**, *7*, 2000853.
(35) (a) Dhass, A. D.; Natarajan, E.; Lakshmi, P. An Investigation of temperature effects on solar photovoltaic cells and modules. *Int. J. Eng., Trans. B* **2014**, *27*, 1713−1722. (b) Sun, C.; Zou, Y.; Qin, C.; Zhang, B.; Wu, X. Temperature effect of photovoltaic cells: a review. *Adv. Compos. Hybrid Mater.* **2022**, *5*, 2675−2699. (c) Al-Ezzi, A. S.; Ansari, M. N. M. Photovoltaic solar cells: A review. *Appl. Syst. Innov.* **2022**, *5*, 67.
(36) Dierking, I. *Textures of Liquid Crystals*; Wiley-VCH Verlag GmbH & Co. KGaA: Weinheim, Germany, 2003; pp 141−144, Chapter 10.
(37) Yelamaggad, C. V.; Achalkumar, A. S.; Rao, D. S. S.; Prasad, S. K. A New Class of Discotic Mesogens Derived from Tris(*N*-salicylideneaniline)s Existing in C_{3h} and C_s Keto-Enamine Forms. *J. Org. Chem.* **2007**, *72*, 8308−8318.
(38) Bisoyi, H. K.; Kumar, S. Carbon nanotubes in triphenylene and rufigallol-based room temperature monomeric and polymeric discotic liquid crystals. *J. Mater. Chem.* **2008**, *18*, 3032−3039.
(39) Achalkumar, A. S.; Yelamaggad, C. V. Light emitting, star-shaped tris(N-salicylideneaniline) discotic liquid crystals bearing trans-stilbene fluorophores: synthesis and characterization. *Tetrahedron Lett.* **2012**, *53*, 7108−7112.
(40) Achalkumar, A. S.; Hiremath, U. S.; Rao, D. S. S.; Prasad, S. K.; Yelamaggad, C. V. Self-assembly of hekates - tris(*N*-salicylideneaniline)s into columnar structures: Synthesis and characterization. *J. Org. Chem.* **2013**, *78*, 527−544.
(41) Achalkumar, A. S.; Veerabhadraswamy, B. N.; Hiremath, U. S.; Rao, D. S. S.; Prasad, S. K.; Yelamaggad, C. V. Photoluminescent discotic liquid crystals derived from tris(N-salicylideneaniline) and stilbene conjugates: Structure-property correlations. *Dyes Pigm.* **2016**, *132*, 291−305.
(42) (a) Kajiyama, T.; Park, K. S.; Usui, F.; Kikuchi, H.; Takahara, A. Phase-separated structure–electro-optical property relationships of polymer/liquid-crystal composite film. *Proc. SPIE* **1993**, *1911*, 122−131. (b) Chigrinov, V. G. *Liquid Crystal Photonics*; Nova Science Pub Inc.: New York, NY, USA, 2014; pp 55−168, Chapter 3, and pp 169−246, Chapter 4. (c) Marinov, Y. G.; Hadjichristov, G. B.; Petrov, A. G.; Prasad, S. K. Thin films of silica nanoparticle doped nematic liquid crystal 7CB for electro-optic modulation. *Photonics Lett. Pol.* **2015**, *7*, 94−96. (d) Marinov, Y. G.; Hadjichristov, G. B.; Petrov, A. G.; Prasad, S. K. Electro-optic modulation by silica-nanostructured nematic system (aerosil/7CB nanocomposite). *Composites, Part B* **2016**, *90*, 471−477. (e) Konshina, E. A.; Shcherbinin, D. P. Study of dynamic light scattering in nematic liquid crystal and its optical, electrical and switching characteristics. *Liq. Cryst.* **2018**, *45*, 292−302. (f) Li, X.; Guo, Y.; Huai, H.; Yang, Y.; Sun, Y.; Zhang, C.; Sun, Y. An electrically controlled light-scattering device based on liquid crystal/polymer microsphere composites. *Liq. Cryst.* **2020**, *47*, 650−657.
(43) (a) Liew, K. M.; Wong, C. H.; He, X. Q.; Tan, M. J. Thermal stability of single and multi-walled carbon nanotubes. *Phys. Rev. B* **2005**, *71*, 075424. (b) Sinha, S. K.; Kumar, D.; Patnaik, A. An investigation on thermal stability of single wall carbon nanotubes (SWCNTs) by molecular dynamics simulations. *Mater. Today: Proc.* **2021**, *44*, 4940−4944.
(44) Yelamaggad, C. V.; Achalkumar, A. S. Tris(N-salicylideneanilines) [TSANs] exhibiting a room temperature columnar mesophase: synthesis and characterization. *Tetrahedron Lett.* **2006**, *47*, 7071−7075.
(45) Li, Q.; Li, L. Photoconducting discotic liquid crystals. In *Thermotropic Liquid Crystals*; Ramamoorthy, A., Ed.; Springer: Dordrecht, The Netherlands, 2007; pp 297−322, Chapter 11.
(46) Monobe, H.; Miyagawa, Y.; Mima, S.; Sugino, T.; Uchida, K.; Shimizu, Y. Photoconductive properties of a mesogenic long-chain tetraphenylporphyrin oxovanadium(IV) complex. *Thin Solid Films* **2001**, *393*, 217−224.
(47) Bushby, R. J.; Donovan, K. J.; Kreouzis, T.; Lozman, O. R. Molecular engineering of tripheynlene-based disotic liquid crystal conductors. *Opto-Electron. Rev.* **2005**, *13*, 269−279.
(48) Jankowiak, A.; Pociecha, D.; Szczytko, J.; Monobe, H.; Kaszyński, P. Photoconductive liquid-crystalline derivatives of 6-oxoverdazyl. *J. Am. Chem. Soc.* **2012**, *134*, 2465−2468.
(49) Kavitha, C.; Avinash, B. S.; Kumar, S.; Lakshminarayanan, V. Photoconductivity of doped hexa-alkoxy triphenylene nano composite structures. *Mater. Chem. Phys.* **2012**, *133*, 635−641.
(50) Bala, I.; De, J.; Pal, S. K.; Govindaraju, T. Functional discotic liquid crystals through molecular self-assembly: Toward efficient charge transport systems. In *Molecular Architectonics and Nanoarchitectonics*; Ariga, K., Ed.; *Springer Series in Nanostructure Science and Technology*; Springer: Singapore, 2022; pp 89−130, Chapter 5.
(51) Balagurusamy, V. S. K.; Prasad, S. K.; Chandrasekhar, S.; Kumar, S.; Manickam, M.; Yelamaggad, C. V. Quasi-one dimensional electrical conductivity and thermoelectric power studies on a discotic liquid crystal. *Pramana* **1999**, *53*, 3−11.
(52) Kastler, M.; Laquai, F.; Müllen, K.; Wegner, G. Room-temperature nondispersive hole transport in a discotic liquid crystal. *Appl. Phys. Lett.* **2006**, *89*, 252103.
(53) (a) Fischer, J. E.; Dai, H.; Thess, A.; Lee, R.; Hanjani, N. M.; Dehaas, D. L.; Smalley, R. E. Metallic resistivity in crystalline ropes of single-wall carbon nanotubes. *Phys. Rev. B: Condens. Matter Mater. Phys.* **1997**, *55*, R4921−R4924. (b) Mann, D.; Javey, A.; Kong, J.; Wang, Q.; Dai, H. Ballistic transport in metallic nanotubes with reliable pd ohmic contacts. *Nano Lett.* **2003**, *3*, 1541−1544. (c) Panhuis, M. I. H. Carbon nanotubes: enhancing the polymer building blocks for intelligent materials. *J. Mater. Chem.* **2006**, *16*, 3598−3605. (d) Maffucci, A.; Maksimenko, S. A.; Miano, G.; Slepyan, G. Y. Electrical conductivity of carbon nanotubes: modeling and characterization. In *Carbon Nanotubes for Interconnects: Process, Design and Applications*; Todri-Sanial, A., Dijon, J., Maffucci, A., Eds.; Springer: Cham, Switzerland, 2017; pp 101−128, Chapter 5.
(54) Dolgov, L.; Kovalchuk, O.; Lebovka, N.; Tomylko, S.; Yaroshchuk, O. Liquid crystal dispersions of carbon nanotubes: dielectric, electro-optical and structural peculiarities. In *Carbon Nanotubes*; Marulanda, J. M., Ed.; IntechOpen: London, UK, 2010; pp 451−484, Chapter 24.
(55) St-Antoine, B.; Menard, D.; Martel, R. Position sensitive photothermoelectric effect in suspended single-walled carbon nanotube films. *Nano Lett.* **2009**, *9*, 3503−3508.
(56) Itkis, M. E.; Borondics, F.; Yu, A.; Haddon, R. C. Bolometric infrared photoresponse of suspended single-walled carbon nanotube films (photoresponse of suspended carbon nanotube networks: single-walled carbon nanotube infrared bolometer). *Science* **2006**, *312*, 413−416.

https://doi.org/10.1021/acsomega.3c02103
ACS Omega 2023, 8, 27102−27116

(57) Qiu, X.; Freitag, M.; Perebeinos, V.; Avouris, P. Photoconductivity spectra of single-carbon nanotubes: implications on the nature of their excited states. *Nano Lett.* **2005**, *5*, 749−752.
(58) Hone, J.; Whitney, M.; Zettl, A. Thermal conductivity of single-walled carbon nanotubes. *Synth. Met.* **1999**, *103*, 2498−2499.
(59) Yu, C.; Shi, L.; Yao, Z.; Li, D.; Majumdar, A. Thermal conductance and thermopower of an individual single-wall carbon nanotube. *Nano Lett.* **2005**, *5*, 1842−1846.
(60) Volkov, A. N.; Zhigilei, L. V. Heat conduction in carbon nanotube materials: Strong effect of intrinsic thermal conductivity of carbon nanotubes. *Appl. Phys. Lett.* **2012**, *101*, 043113.
(61) Zhigilei, L. V.; Salaway, R. N.; Wittmaack, B. K.; Volkov, A. N. Computational studies of thermal transport properties of carbon nanotube materials. In *Carbon Nanotubes for Interconnects: Process, Design and Applications*; Todri-Sanial, A., Dijon, J., Maffucci, A., Eds.; Springer: Cham, Switzerland, 2016; pp 129−161, Chapter 6.
(62) Kumanek, B.; Janas, D. Thermal conductivity of carbon nanotube networks: a review. *J. Mater. Sci.* **2019**, *54*, 7397−7427.
(63) Jorio, A.; Dresselhaus, G.; Dresselhaus, M. S. *Physical Properties of Carbon Nanotubes*; Imperial College Press: London, UK, 1998.
(64) Dehghani, S.; Moravvej-Farshi, M. K.; Sheikhi, M. H. Temperature dependence of electrical resistance of individual CNT and CNT network. *Mod. Phys. Lett. B* **2012**, *26*, 1250136.
(65) Dehghani, S.; Moravvej-Farshi, M. K.; Sheikhi, M. H. Compact formulas for the electrical resistance of semiconducting and metallic single wall carbon nanotubes. *Fullerenes, Nanotubes Carbon Nanostruct.* **2015**, *23*, 899−905.
(66) Podlesny, B.; Kumanek, B.; Borah, A.; Yamaguchi, R.; Shiraki, T.; Fujigaya, T.; Janas, D. Thermoelectric properties of thin films from sorted single-walled carbon nanotubes. *Materials* **2020**, *13*, 3808.
(67) Simmons, T. J.; Vera-Reveles, G.; Gonzalez, G.; Gutierrez-Hernandez, J. M.; Linhardt, R. J.; Navarro-Contreras, H.; Gonzalez, F. J. Bolometric properties of semiconducting and metallic single-walled carbon nanotube composite films. *ACS Photonics* **2015**, *2*, 334−340.
(68) Vera-Reveles, G.; Simmons, T. J.; Bravo-Sanchez, M.; Vidal, M. A.; Navarro-Contreras, H.; Gonzalez, F. J. High-sensitivity bolometers from self-oriented single-walled carbon nanotube composites. *ACS Appl. Mater. Interfaces* **2011**, *3*, 3200−3204.
(69) Cech, J.; Swaminathan, V.; Wijewarnasuriya, P.; Currano, L. J.; Kovalskiy, A.; Jain, H. Fabrication of freestanding SWCNT networks for fast microbolometric focal plane array sensor. *Proc. SPIE* **2010**, *7679*, 76792N1−76792N6.
(70) Kedzierski, K.; Rytel, K.; Barszcz, B.; Gronostaj, A.; Majchrzycki, L.; Wrobel, D. On the temperature dependent electrical resistivity of CNT layers in view of variable range hopping models. *Org. Electron.* **2017**, *43*, 253−261.
(71) Mustonen, T.; Mäklin, J.; Kordás, K.; Halonen, N.; Tóth, G.; Saukko, S.; Vähäkangas, J.; Jantunen, H.; Kar, S.; Ajayan, P. M.; Vajtai, R.; Helistö, P.; Seppä, H.; Moilanen, H. Controlled Ohmic and nonlinear electrical transport in inkjet-printed single-wall carbon nanotube films. *Phys. Rev. B: Condens. Matter Mater. Phys.* **2008**, *77*, 125430.
(72) Benoit, J. M.; Corraze, B.; Chauvet, O. Localization, coulomb interactions, and electrical heating in single-wall carbon nanotubes/polymer composites. *Phys. Rev. B: Condens. Matter Mater. Phys.* **2002**, *65*, 241405−241408.
(73) Aliev, A. E. Bolometric detector on the basis of single-wall carbon nanotube/polymer composite. *Infrared Phys. Technol.* **2008**, *51*, 541−545.
(74) Han, Z. J.; Ostrikov, K. Controlled electronic transport in single-walled carbon nanotube networks: Selecting electron hopping and chemical doping mechanisms. *Appl. Phys. Lett.* **2010**, *96*, 233115.
(75) Yanagi, K.; Udoguchi, H.; Sagitani, S.; Oshima, Y.; Takenobu, T.; Kataura, H.; Ishida, T.; Matsuda, K.; Maniwa, Y. Transport mechanisms in metallic and semiconducting single-wall carbon nanotube networks. *ACS Nano* **2010**, *4*, 4027−4032.
(76) Skakalova, V.; Kaiser, A. B.; Woo, Y. S.; Roth, S. Electronic transport in carbon nanotubes: From individual nanotubes to thin and thick networks. *Phys. Rev. B: Condens. Matter Mater. Phys.* **2006**, *74*, 085403.
(77) Kaiser, A. B.; Skakalova, V. Electronic conduction in polymers, carbon nanotubes and graphene. *Chem. Soc. Rev.* **2011**, *40*, 3786−3801.
(78) Hu, L.; Hecht, D. S.; Grüner, G. Percolation in transparent and conducting carbon nanotube networks. *Nano Lett.* **2004**, *4*, 2513−2517.
(79) Unalan, H. E.; Fanchini, G.; Kanwal, A.; Du Pasquier, A.; Chhowalla, M. Design criteria for transparent single-wall carbon nanotube thin-film transistor. *Nano Lett.* **2006**, *6*, 677−682.
(80) Naeemi, A.; Meindl, J. D. Physical modeling of temperature coefficient of resistance for single- and multi-wall carbon nanotube interconnects. *IEEE Electron Device Lett.* **2007**, *28*, 135−138.
(81) Lu, R.; Xu, G.; Wu, J. Z. Effects of thermal annealing on noise property and temperature coefficient of resistance of single-walled carbon nanotube films. *Appl. Phys. Lett.* **2008**, *93*, 213101.
(82) Kordás, K.; Tóth, G.; Moilanen, P.; Kumpumäki, M.; Vähäkangas, J.; Uusimäki, A.; Vajtai, R.; Ajayan, P. M. Chip cooling with integrated carbon nanotube microfin architectures. *Appl. Phys. Lett.* **2007**, *90*, 123105.
(83) Fu, Y.; Nabiollahi, N.; Wang, T.; Wang, S.; Hu, Z.; Carlberg, B.; Zhang, Y.; Wang, X.; Liu, J. A complete carbon-nanotube-based on-chip cooling solution with very high heat dissipation capacity. *Nanotechnology* **2012**, *23*, 045304.
(84) Mäklin, J. *Electrical and Thermal Applications of Carbon Nanotube Films*; University of Oulu, 2014.

https://doi.org/10.1021/acsomega.3c02103
ACS Omega 2023, 8, 27102−27116